

1 **Proteolytically released Lasso/teneurin-2 induces axonal**
2 **attraction by interacting with latrophilin-1 on axonal growth**
3 **cones**

4 Nickolai V. Vysokov^{1,2,3,4}, John-Paul Silva^{2,5}, Vera G. Lelianova^{1,2}, Jason Suckling^{2,6}, John
5 Cassidy^{2,7}, Jennifer K. Blackburn^{1,8}, Natalia Yankova^{2,9}, Mustafa B.A. Djamgoz², Serguei V.
6 Kozlov¹⁰, Alexander G. Tonevitsky^{11,12}, Yuri A. Ushkaryov^{1,2,13,*}

7 ¹School of Pharmacy, University of Kent, Chatham, ME4 4TB, UK

8 ²Department of Life Sciences, Imperial College London, London, SW7 2AZ, UK

9 ³Wolfson Centre for Age Related Diseases, King's College London, London SE1 1UL, UK

10 ⁴BrainPatch Ltd., 3 Gower Street, London, WC1E 6HA, UK

11 ⁵Department of Bioanalytical Sciences, Non-clinical development, UCB-Pharma, Slough,
12 Berkshire, SL1 3WE, UK

13 ⁶Thomsons Online Benefits, Gordon House, 10 Greencoat Place, SW1P 1PH, London, UK

14 ⁷Arix Bioscience, London, W1J 6EQ, UK

15 ⁸Division of Molecular Psychiatry, Yale University School of Medicine, New Haven, CT 06510,
16 USA

17 ⁹Institute of Psychiatry, Psychology & Neuroscience, Maurice Wohl Clinical Neuroscience
18 Institute, Department of Basic and Clinical Neuroscience, King's College London, London SE5
19 9NU, UK

20 ¹⁰Center for Advanced Preclinical Research, National Cancer Institute, Frederick, MD 21702, USA

21 ¹¹Higher School of Economics, 20 Myasnitskaya, Moscow, 101000, Russia

22 ¹²Scientific Research Centre Bioclinicum, Moscow, 115088, Russia.

23 ¹³Lead Contact

24 *Correspondence: y.ushkaryov@kent.ac.uk

25 **Running title: Cleaved Lasso Attracts Axons via latrophilin-1**

26 **ABSTRACT**

27 A presynaptic adhesion G-protein-coupled receptor, latrophilin-1, and a postsynaptic
28 transmembrane protein, Lasso/teneurin-2, are implicated in trans-synaptic interaction that
29 contributes to synapse formation. Surprisingly, during neuronal development, a substantial
30 proportion of Lasso is released into the intercellular space by regulated proteolysis, potentially
31 precluding its function in synaptogenesis. We found that released Lasso binds to cell-surface
32 latrophilin-1 on axonal growth cones. Using microfluidic devices to create stable gradients of
33 soluble Lasso, we show that it induces axonal attraction, without increasing neurite outgrowth.
34 Using latrophilin-1 knockout in mice, we demonstrate that latrophilin-1 is required for this effect.
35 After binding latrophilin-1, Lasso causes downstream signaling, which leads to an increase in
36 cytosolic calcium and enhanced exocytosis, processes that are known to mediate growth cone
37 steering. These findings reveal a novel mechanism of axonal pathfinding, whereby latrophilin-1
38 and Lasso mediate both short-range interaction that supports synaptogenesis, and long-range
39 signaling that induces axonal attraction.

40

41 Keywords: axon attraction / axon guidance / Lasso / latrophilin / teneurin-2

42

43 INTRODUCTION

44 Correct wiring of the nervous system critically depends on both long-range diffusible cues and
45 short-range contact-mediated factors which can be attractive or repulsive (Chen and Cheng,
46 2009). However, the relatively small repertoire of key molecules known to be involved in axon
47 guidance or trans-synaptic adhesion cannot fully explain the complexity and specificity of synaptic
48 connections. Indeed, new interacting partners and signal-modulating ligands are now being found
49 for many well-established guidance factors (Karaulanov et al., 2009; Leyva-Diaz et al., 2014;
50 Sollner and Wright, 2009). Furthermore, our novel findings demonstrate that at least one receptor
51 pair can both mediate cell contacts and, unexpectedly, also act as a long-range signaling factor
52 and its receptor.

53 This trans-synaptic receptor pair consists of presynaptic latrophilin-1 (LPHN1) and postsynaptic
54 Lasso (Silva et al., 2011). LPHN1 (also known as ADGRL1 for *Adhesion G-protein-coupled*
55 *Receptor, Latrophilin subfamily 1* (Hamann et al., 2015)) is a cell-surface receptor that is
56 expressed by all central neurons (Davletov et al., 1998; Ichtchenko et al., 1999; Matsushita et al.,
57 1999; Sugita et al., 1998). An array of data indicates that LPHN1 is localized on axons, axonal
58 growth cones and nerve terminals (Silva et al., 2011). Activation of LPHN1 by its agonist, mutant
59 latrotoxin (LTX^{N4C}), stimulates vesicular exocytosis (Ashton et al., 2001; Lajus et al., 2006;
60 Lelyanova et al., 2009; Silva et al., 2009; Tobaben et al., 2002; Volynski et al., 2003; Deák et al.,
61 2009). LPHN1 knockout (KO) in mice leads to abnormal rates of embryonic lethality and psychotic
62 phenotypes (Tobaben et al., 2002), indicating the importance of LPHN1 in early development and
63 in cognitive functions in adulthood.

64 The second member of this receptor pair, Lasso, is a representative of teneurins (TENs), large
65 single-pass transmembrane proteins (Baumgartner et al., 1994; Levine et al., 1994). Lasso is the
66 splice variant of TEN2 (TEN2-SS) (Figure 1A) that specifically binds LPHN1 in cell adhesion

67 experiments (Li et al., 2018). Given also that only Lasso is isolated by affinity chromatography on
68 LPHN1 (Silva et al., 2011), we will refer here to TEN2 that is able to bind LPHN1 as Lasso. All
69 TENs possess a large C-terminal extracellular domain (ECD) containing a series of epidermal
70 growth factor (EGF)-like repeats and other repeat domains (Figure 1A). Inter-chain disulfide
71 bridges mediate TEN homodimerization (Figure 1B, left) (Feng et al., 2002; Vysokov et al., 2016).
72 Similar to Notch, during the intracellular processing of TENs, their ECDs are constitutively cleaved
73 by furin at site 1 (Figure 1A, B, left) (Rubin et al., 1999; Tucker and Chiquet-Ehrismann, 2006;
74 Vysokov et al., 2016). However, the cleaved ECD remains tightly tethered to the cell surface due
75 to its strong interaction with the transmembrane fragment (Figure 1B, middle) (Vysokov et al.,
76 2016).

77 TENs have been implicated in promoting axon guidance and neurite outgrowth (Minet et al., 1999;
78 Rubin et al., 1999; Antinucci et al., 2013; Leamey et al., 2007; Young et al., 2013; Hor et al.,
79 2015). For example, different TENs can mediate neuronal cell adhesion (Boucard et al., 2014;
80 Rubin et al., 2002; Silva et al., 2011). TEN2 and TEN4, which are present on dendritic growth
81 cones and developing filopodia, may be responsible for dendritic spine formation (Rubin et al.,
82 1999; Suzuki et al., 2014), while substrate-attached TEN1 supports neurite growth (Minet et al.,
83 1999). However, a mechanistic insight into the role of TENs in axonal growth is still lacking.

84 One possibility is that TENs, as *bona fide* cell-surface receptors, could bind other cell-surface
85 molecules and thus mediate axonal pathfinding. TENs can form homophilic complexes (Rubin et
86 al., 2002; Beckmann et al., 2013). However, TENs failed to mediate homophilic cell adhesion in
87 direct experiments (Boucard et al., 2014; Li et al., 2018). In addition, homophilic interactions of a
88 recombinant soluble TEN2 ECD with the cell-surface TEN2 inhibited (rather than promoted)
89 neurite outgrowth (Beckmann et al., 2013; Young et al., 2013). By contrast, heterophilic
90 interactions of TENs can promote synapse formation (Mosca et al., 2012; Silva et al., 2011). More
91 specifically, heterophilic interaction between Lasso and LPHN1, its strongest ligand (Silva et al.,

92 2011; Boucard et al., 2014), consistently mediates cell adhesion (Silva et al., 2011; Boucard et
93 al., 2014; Le et al., 2018) and is thought to facilitate synapse formation (Silva et al., 2011).

94 However, our surprising finding (Vysokov et al., 2016) that Lasso/TEN2 is partially released from
95 the cell surface by regulated proteolysis (at site 3; Figure 1B, right) was inconsistent with a cell-
96 surface function of Lasso. On the other hand, we found that the released Lasso fragment retained
97 its ability to bind cell-surface LPHN1 with high affinity and induce intracellular signaling (Silva et
98 al., 2011; Vysokov et al., 2016). Thus, it was possible that the released, soluble ECD of
99 Lasso/TEN2 could act as a diffusible (attractive or repulsive) factor and mediate some of the
100 TEN2 functions in neurite pathfinding described above. Therefore, we hypothesized that the
101 binding of soluble Lasso to LPHN1 on distant neurites could trigger important changes in their
102 growth.

103 We tested this hypothesis using cultured hippocampal neurons. First, we show that developing
104 neurons release a substantial proportion of Lasso ECD into the medium, while LPHN1 is
105 concentrated on the leading edge of axonal growth cones. We then use microfluidic chambers to
106 demonstrate that a spatio-temporal gradient of soluble Lasso attracts neuronal axons, but not
107 dendrites, and that this process involves LPHN1 that is present on axonal growth cones. Using
108 model cells expressing functional LPHN1, and mouse neuromuscular preparations, we also show
109 that LPHN1 activation by soluble Lasso causes intracellular Ca^{2+} signaling, which leads to
110 increased exocytosis. This suggests a plausible cellular mechanism causing axons to turn in the
111 direction of a gradient of soluble Lasso. Moreover, the LPHN1-Lasso pair illustrates a novel
112 principle of chemical guidance whereby cell-surface receptors engage not only in short-range
113 interactions, but also in long-range signaling, which can further contribute to the formation of
114 complex neuronal networks.

115 **RESULTS**

116 **Neurons partially cleave and release Lasso**

117 We previously showed in model cell lines and in adult brain that Lasso is cleaved at several sites
118 (sites 1, 2, 3 in Figure 1A, B) and is released into the extracellular environment in a regulated
119 manner (Vysokov et al., 2016). To test whether Lasso undergoes the same processing and
120 release during neuronal development, we followed Lasso expression at different stages of neuron
121 maturation in hippocampal cell cultures (Kaech and Banker, 2006). Soon after plating, embryonic
122 (E18) rat hippocampal neurons produced Lasso, which was detectable at 3 days *in vitro* (DIV)
123 (Figure 1C, D). A large proportion of Lasso (~90%) was constitutively cleaved at site 1 during
124 neuronal development *in vitro* (Figure S1A). Increasing amounts of cleaved fragment also
125 appeared in the medium at 7 and 14 DIV (Figure 1D and S1A, green), indicating a slow cleavage
126 at site 3. Thus, Lasso is fully cleaved at site 1 and partially released by regulated cleavage at site
127 3 not only in transfected immortalized cells, but also in developing neurons and in the postnatal
128 rat brain (Vysokov et al., 2016).

129 We also examined the neuronal structures that could release soluble Lasso ECD. We found that
130 large amounts of Lasso were present on dendrites and dendritic growth cones (Figure S1B), while
131 it was practically absent from axons and axonal growth cones (Figure 1E). Since about 80% of
132 Lasso was not normally released (Figure 1D, S1A), these data suggested that the compartments
133 rich in Lasso, i.e. dendrites and dendritic growth cones, were the main source of the soluble Lasso
134 fragment.

135 **LPHN1 is expressed on growth cones of developing neurons**

136 As early as 3 DIV, the developing neurons also expressed LPHN1, the high-affinity receptor for
137 soluble Lasso ECD, and the amounts of LPHN1 continued to increase through all time points (Fig
138 1B), in parallel with the increasing amounts of soluble Lasso (Fig S1A). This correlation between

139 the soluble Lasso and cell-surface LPHN1 further supported the idea of their likely interaction
140 during neuronal development.

141 Interestingly, in developing hippocampal neurons, LPHN1 was found concentrated in axons and
142 especially in axonal growth cones, where it co-localized with synapsin (Figure S1C, D,
143 arrowheads). LPHN1 was also enriched in axonal varicosities, which were identified as *en*
144 *passant* synapses by immunostaining for PSD-95 (Figure S1D, asterisks).

145 We then studied the expression of LPHN1 in growth cones in more detail by transfecting
146 hippocampal neurons with GFP, which greatly simplified the identification and tracking of axons
147 and axonal growth cones. All GFP-labeled axonal growth cones showed a clear enrichment of
148 endogenous LPHN1 (Figure 1F, G, I). Conversely, when LPHN1 expression was knocked down
149 by shRNA (delivered together with GFP in the same bicistronic vector), it clearly disappeared from
150 the growth cones of transfected neurons, while the growth cones of non-transfected cells were
151 not affected (Figure S1E, arrow and arrowhead, respectively).

152 We also discovered that endogenous LPHN1 expression within axonal growth cones was
153 polarized in relation to the cone's symmetry axis, such that one side of each growth cone
154 contained on average 1.88 ± 0.22 fold more LPHN1 than the other (Figure 1G, H). To assess
155 whether this LPHN1 enrichment correlated with the direction of axonal growth, we traced the
156 growth trajectories of a number of symmetrical growth cones and compared these with the
157 distribution of LPHN1. This analysis clearly demonstrated that LPHN1 polarization within the
158 growth cones very strongly positively correlated with the direction of their turning (Figure 1G, H).
159 Moreover, in non-symmetrical growth cones, which had clearly started turning prior to fixation,
160 LPHN1 expression had a bimodal distribution, being enriched not only near the "neck" of a turning
161 cone, but also close to its leading edge (Figure S1F, G). Such leading-edge enrichment also
162 extended into fine growth cone protrusions. Thus, filopodia and lamellipodia located on the

163 leading edge of a growth cone (Figure 1I, left, arrowheads) showed a much higher amount of
164 LPHN1 than the processes on the trailing edge of the growth cone (Figure 1I, right).

165 We concluded that LPHN1 expression within growth cones correlated positively with the global
166 directionality of growth and with the fine structures that underpin the growth cone's extension.

167 **Soluble Lasso binds to cell-surface LPHN1**

168 Next, we tested the interaction between soluble Lasso and cell-surface LPHN1. For these tests
169 we expressed a shorter, constitutively secreted construct, Lasso-D (Figure 2A, right) in HEK293A
170 cells and affinity-purified it (Figure 2B). 100 nM Lasso-D was incubated with neuroblastoma cells
171 stably expressing (i) LPHN1, (ii) a chimeric construct LPH-82 containing ECD from EMR-2 used
172 as a negative control, (iii) Lasso-A, or (iv) Lasso-FS (Figure 2A, left). As expected, Lasso-D did
173 not interact with LPH-82 (Figure 2C, panel 4). The lack of Lasso-D binding to Lasso-A and
174 released fragment of Lasso-A binding to Lasso-FS (Figure 2D, panels 2, 3; Figure 2—supplement
175 1, B) was somewhat surprising, since homophilic interactions between membrane-bound and
176 soluble TENs were reported previously (Bagutti et al., 2003; Beckmann et al., 2013; Hong et al.,
177 2012; Rubin et al., 2002; Boucard et al., 2014), but this could be due to a relatively low affinity of
178 Lasso-Lasso interaction and relatively long washes employed in our protocol. On the other hand,
179 and consistent with previous reports of high affinity between LPH1 and Lasso (Silva et al., 2011;
180 Boucard et al., 2014), Lasso-D and the released fragment of Lasso-A bound strongly to cells
181 expressing LPHN1 (Figure 2C, panels 2, 3 and Figure 2—supplement 1, A).

182 To verify that the soluble ECD of Lasso, when proteolytically released from the cell-surface as
183 depicted in Figure 2A (Lasso-A), could diffuse between individual cells and bind LPHN1 on distant
184 cells, we co-cultured neuroblastoma cells stably expressing Lasso-A with cells stably expressing
185 LPHN1. When co-cultured at high density, these cells formed clusters, held together by

186 LPHN1/Lasso-A intercellular adhesion complexes (Fig 2E, panel 1). In more sparsely plated co-
187 cultures, the Lasso-A fragment was released into the medium, where it diffused and bound to
188 cells expressing LPHN1, but not to the wild type (WT) neuroblastoma cells (Figure 2E, panel 2,
189 and Figure 2—supplement 1, C). Interestingly, after binding Lasso, the LPHN1 staining appeared
190 to concentrate in large patches, a pattern very different from LPHN1 distribution in control
191 conditions (Figure 2C, panel 1) (see also below). These experiments suggest that (i) when Lasso
192 is released into the medium as a result of its regulated cleavage, it retains its affinity for LPHN1
193 and (ii) on reaching distant LPHN1-expressing cells by diffusion, Lasso causes LPHN1
194 redistribution on the cell surface.

195 We then asked whether the soluble Lasso ECD could similarly bind to LPHN1 in neurons and,
196 more specifically, on axonal growth cones. To control for the specificity of Lasso binding to
197 LPHN1, this experiment was carried out on cultured hippocampal neurons from LPHN1 WT
198 (*Adgr11^{+/+}*) and LPHN1 KO (*Adgr11^{-/-}*) newborn mice (P0). Also, to unequivocally distinguish
199 between the soluble and cell-surface Lasso, we used exogenous Lasso-D, which was detected
200 using anti-FLAG antibody. As expected, in WT mouse neurons, LPHN1 was found mostly in
201 axonal growth cones (arrowheads) and varicosities (asterisks) (Figure 2—supplement 2, A,
202 green). The exogenous Lasso-D clearly bound to these structures (Figure 2—supplement 2, A,
203 red; C), but in general did not interact with dendrites. By contrast, the axons and growth cones of
204 LPHN1 KO neurons did not show specific LPHN1 staining and appeared unable to bind the
205 soluble exogenous Lasso-D (Figure 2—supplement 2, B, C). These results indicated that
206 released Lasso ECD could interact with LPHN1 on axonal growth cones.

207 **MAIDs as a tool to study axonal responses to chemoattractant gradients**

208 Based on the data above, we hypothesized that the interaction of released Lasso ECD with
209 LPHN1 on axonal growth cones could represent one of the mechanisms that underlie the

210 previously formulated, but so far unexplained, role of TENs in axonal pathfinding and brain
211 patterning (Antinucci et al., 2013; Hor et al., 2015; Leamey et al., 2007; Young et al., 2013). To
212 study this effect, we developed a new method of long-term exposure of hippocampal axons to
213 stable gradients of Lasso using “microfluidic axon isolation devices” (MAIDs) (Figure 3A). The
214 advantage of this method over conventional ligand-puffing was that the MAIDs enabled exposure
215 of axons to long-term stable gradients of Lasso, which was critical for our assay. The device used
216 here had two compartments, each consisting of two cylindrical wells connected by a “corridor”; a
217 150 μm -thick wall that separated the two corridors had multiple parallel microchannels (2-3 μm
218 tall and 10 μm wide) connecting the two compartments (Figure 3A, middle). When neurons are
219 plated in one of the compartments (designated as the Somal Compartment), their neurites grow
220 in all directions, but only the axons (identified by NF-H staining) readily penetrate the
221 microchannels and cross into the empty, Axonal Compartment (Figure 3A, right; 3B, C). While
222 there is a large number of dendrites in the Somal Compartment (identified by microtubule-
223 associated protein 2, MAP-2, staining), only a few of them enter the Axonal Compartment and
224 then terminate close to the wall (Figure 3B, C).

225 From the previously described physical characteristic of microfluidic chambers (Zicha et al.,
226 1991), we predicted that a concentration gradient across the microchannels in our devices could
227 be established over time. This was modelled by adding TRITC-conjugated BSA to one
228 compartment and visualizing the dye in the microchannels (Figure 3D). We found that a gradient
229 was formed within the first 24 h and remained stable over several days (Figure 3D, E).

230 To test the functionality of the MAIDs for studying axonal guidance, we employed brain-derived
231 neurotrophic factor (BDNF) known to act as an axonal chemoattractant (Li et al., 2005). Rat
232 hippocampal neurons were plated into the Somal Compartment, and at 3 DIV, when axons
233 normally start entering microchannels, BDNF was added to the Axonal Compartment (PBS was
234 added to control cultures) (Figure 3F). After a further 5 DIV, we observed a 2.2-fold higher number

235 of axons crossing into the Axonal Compartment in the presence of BDNF compared with the
236 control (Figure 3G, H). This effect was statistically significant (Figure 3H). This proof-of-concept
237 experiment confirmed that MAIDs could be used to study the long-term effects of chemoattractant
238 gradients on axonal migration.

239 **A gradient of soluble Lasso induces axonal attraction**

240 We then used this methodology to study the reaction of LPHN1-expressing neuronal growth
241 cones to a gradient of soluble released Lasso. Lasso-D was added to the Axonal Compartment
242 (Figure 4A), and the integrity of Lasso during the experiment was verified by Western blotting
243 (Figure 4B). Quantification of axons in Axonal Compartments by NF-H immunofluorescence
244 (Figure 4C, D) revealed a statistically significant 1.5-fold increase in axonal growth induced by
245 Lasso-D. Thus, soluble Lasso-D clearly functioned as an attractant of axonal elongation and/or
246 steering.

247 Since LPHN1 is present on axonal growth cones (Figs. 1, S1), binds soluble Lasso (Figure 2,
248 Figure 2—supplement 1) and is the strongest interacting partner of Lasso (Boucard et al., 2014;
249 Silva et al., 2011), we hypothesized that LPHN1 may be involved in the observed Lasso-mediated
250 attraction of axons (Figure 4—supplement 1, A). To investigate this, hippocampal cultures from
251 LPHN1 KO or WT mice (genotyping shown in Figure 4—supplement 1, B) were exposed to a
252 gradient of Lasso-D added to the Axonal Compartment. The total amount of neurites and cells in
253 both compartments were quantified using the lipophilic membrane tracer DiO (see Methods for
254 details). The results clearly demonstrated that the neurites from LPHN1-expressing (WT)
255 hippocampal neurons crossed into the Lasso D-containing Axonal Compartment 5.5-fold more
256 readily than the neurites from neurons lacking this receptor (Figure 4E, left). Importantly, this
257 effect was not due to a lower viability of LPHN1 KO neurons, because there was no difference
258 between the KO and WT cells within the Somal Compartment (Figure 4E, right).

259 We also studied the behavior of axons in response to a spatio-temporal Lasso gradient in the
260 corridor of the Axonal Compartment, by exposing axons to an increasing concentration of the
261 attractant during the whole growth process. In order to achieve a stable increase in protein
262 concentration over time, we seeded HEK293A cells stably expressing soluble Lasso-D
263 (untransfected HEK293A cells were used in control) into the wells of the Axonal Compartment
264 (Figure 5A). The presence of secreted Lasso-D within the Axonal Compartments was verified at
265 the end of each experiment (Fig 5B), and the distribution of axons was quantified by NF-H
266 immunofluorescence (Figure 5C, D). In this experiment, we observed not only a significantly
267 greater number of axons being attracted, but also axons growing deeper into the corridors of the
268 Axonal Compartments (Figure 5D). On the other hand, quantification of MAP-2
269 immunofluorescence demonstrated that released Lasso-D did not attract dendrites; in fact, there
270 was a slight repulsive effect (Figure 5E). Taken together, these experiments indicate that a
271 gradient of the soluble Lasso fragment specifically induces axonal attraction.

272 Soluble Lasso fragment also induced strong axonal fasciculation (e.g. Figure 4C and 5C). This
273 effect was quantified by measuring the width of axonal bundles at 100 μm from the separating
274 wall, where axons grew mostly away from the wall rather than along it. Based on the average
275 width of a single axon (1 μm), an average bundle contained 2-3 axons in control conditions, but
276 more than 5 axons in the presence of 1.5 nM Lasso-D (Figure 5F). Thus, Lasso fragment can
277 induce axonal fasciculation in a concentration-dependent manner.

278 In order to rule out the possibility that the observed effects of the released Lasso fragment were
279 due to a general positive trophic effect (e.g. an increase in axonal elongation speed), Lasso-D
280 was added directly to cultures of hippocampal neurons. To visualize axons, neurons were
281 transfected with GFP prior to plating and allowed to grow for 4 DIV, after which the longest
282 neurites of GFP-positive neurons were traced and measured. We did not detect any increase in
283 the length of neurites when neurons were exposed to Lasso-D (Figure 5G, H).

284 Taken together, these data demonstrate unequivocally that a gradient of the soluble fragment of
285 Lasso acts as an axonal attraction cue without affecting their overall growth.

286 **The mechanism of axonal attraction by Lasso**

287 To determine the downstream effects of the interaction between soluble Lasso ECD and LPHN1,
288 we used neuroblastoma cells stably expressing LPHN1. It was reported previously that the
289 signaling machinery downstream of LPHN1 in these cells is similar to that in neurons (Silva et al.,
290 2009; Volynski et al., 2004). When the LPHN1-expressing neuroblastoma cells are stimulated by
291 the known LPHN1 ligand and potent secretagogue LTX^{N4C}, the N-terminal and C-terminal
292 fragments (NTF and CTF) of LPHN1 undergo rearrangement (as illustrated in Figure 6A, middle).
293 In turn, this induces intracellular Ca²⁺ signaling which involves the activation of Gα_q and
294 phospholipase C (PLC), and release of inositol 1,4,5-trisphosphate (IP₃) (Silva et al., 2009;
295 Volynski et al., 2004).

296 These observations suggested that Lasso might also affect the distribution of NTF and CTF of
297 LPHN1 in the plasma membrane. Indeed, we noticed that soluble Lasso-D or Lasso-A caused
298 the NTF to aggregate into patches on the surface (Figure 2C, panel 2; Figure 2—supplement 1,
299 C). To test whether Lasso also causes a redistribution of the CTF required for intracellular
300 signaling, we applied Lasso-D to LPHN1-expressing cells and followed the fate of both NTF and
301 CTF. We observed a dramatic rearrangement of both LPHN1 fragments in the membrane, leading
302 to the formation of large molecular aggregates also containing Lasso (Figure 6C). Similar
303 clustering of both LPHN1 fragments was also induced by LTX^{N4C}, a strong LPHN1 agonist (Figure
304 6D). On the other hand, an antibody recognizing the V5 epitope at the N-terminus of NTF only
305 caused NTF clustering, but did not affect the distribution of CTF (Figure 6A, right; Figure 6E).
306 Thus, soluble Lasso ECD, which causes the association of the LPHN1 fragments, might be a
307 functional agonist of LPHN1, similar to LTX^{N4C}. By analogy, this also indicated that the soluble

308 Lasso fragment could induce signal transduction via the CTF of LPHN1 coupled to a G-protein.

309 The effect of LTX^{N4C} can be assessed by monitoring cytosolic Ca²⁺ (Silva et al., 2011; Volynski et
310 al., 2004). We therefore investigated whether the soluble Lasso ECD could induce similar effects.
311 LPH1-expressing neuroblastoma cells were stimulated with saturating concentrations of Lasso-
312 D, LTX^{N4C} (positive control) or buffer (negative control), while cytosolic calcium levels were
313 monitored using an intracellular Ca²⁺-sensing dye, Fluo-4 (see Figure 7—figure supplement 1, A
314 for the scheme of experiment). Similar to LTX^{N4C}, in the absence of extracellular Ca²⁺, Lasso-D
315 did not cause any Ca²⁺ signals in LPHN1-expressing NB2a cells (Figure 7A). However, when
316 extracellular Ca²⁺ was added to the cells, the rise in intracellular Ca²⁺ signal was significantly
317 higher in the presence of the ECD of Lasso, compared to negative control (Figure 7A). Thus,
318 Lasso-D is able to cause intracellular Ca²⁺ signaling in LPHN1-expressing cells.

319 One of the features of LTX^{N4C}-induced effects (such as Ca²⁺ signaling and neurotransmitter
320 release) is that they develop with a delay of ~20 minutes, which has been attributed to the time
321 taken by the toxin to assemble the LPHN1 fragments together and cause its maximal activation
322 (Volynski et al., 2004). We predicted, therefore, that the rearrangement of the NTF and CTF
323 induced by soluble Lasso (Figure 6C) should prepare the signaling machinery for stimulation by
324 the toxin. To test this idea, we first treated the LPHN1-expressing cells with Lasso-D and then
325 with LTX^{N4C} (Figure 7—figure supplement 1, B). When Lasso-D was applied in the presence of 2
326 mM Ca²⁺, it induced relatively short-lived intracellular Ca²⁺ signaling (Figure 7B, right, prior to the
327 blue arrowhead). However, when LTX^{N4C} was then added, it triggered Ca²⁺ signaling after a
328 shorter delay (~14 min), instead of the usual ~23 min (Figure 7C). This additivity of effects is
329 consistent with soluble Lasso inducing intracellular Ca²⁺ signaling via the same molecular
330 mechanism as LTX^{N4C}.

331 Another well-known effect of LTX^{N4C} is the burst-like release of neurotransmitters, linked to the

332 elevated levels of cytosolic Ca^{2+} (Lelyanova et al., 2009; Volynski et al., 2003). As Lasso-D
333 likewise increased intracellular Ca^{2+} concentration, it might also trigger such transmitter
334 exocytosis. To test this hypothesis, we applied a previously characterized (Silva et al., 2011),
335 soluble, short C-terminal Lasso construct (Lasso-G, Figure 1A) to mouse neuromuscular
336 preparations and recorded the spontaneous miniature end plate potentials (MEPPs), which
337 correspond to individual exocytotic events. We found that incubation with Lasso-G significantly
338 increased MEPPs frequency from 1.61 ± 0.27 Hz in control to 3.83 ± 0.79 Hz in the presence of
339 Lasso-G (Figure 7D, E). However, this was much less than the effect of LTX^{N4C} , which triggered
340 massive secretion of neurotransmitter reaching 29.5 ± 4.1 Hz (Figure 7F). To ascertain that both
341 these effects were mediated by LPHN1, we used neuromuscular preparations from LPHN1 KO
342 mice. Interestingly, unstimulated LPHN1 KO motor neurons showed an increased MEPPs
343 frequency compared to synapses from WT animals (3.33 ± 0.79 Hz in KO synapses). However,
344 neither Lasso-G, nor LTX^{N4C} had any effect on exocytosis in preparations lacking LPHN1 (Figure
345 7E, F; 3.4 ± 0.68 Hz with Lasso-G and 3.8 ± 1.4 Hz with LTX^{N4C}). In all the recordings, the mean
346 *amplitudes* of MEPPs under any condition did not differ significantly (Figure 7—figure supplement
347 1, C), which indicated a purely presynaptic effect of the two LPHN1 agonists and of LPHN1
348 ablation. These results show that the soluble Lasso fragment can increase exocytosis at nerve
349 terminals, and confirm the importance of LPHN1 in the observed effects of LTX and the ECD of
350 Lasso.

351 From the results reported here, we hypothesize that the soluble Lasso fragment, released by
352 developing neurons, interacts with LPHN1 on axonal growth cones and nerve terminals. It then
353 causes clustering of LPHN1 fragments and activation of downstream signaling, causing an
354 increase in cytosolic Ca^{2+} and subsequent exocytosis. The latter two processes are known to be
355 key regulators of axonal attraction (Tojima et al., 2011). Thus, the ability of soluble Lasso to
356 activate these processes on axonal growth cones could underpin the mechanisms by which it

357 attracts axons.

358 **DISCUSSION**

359 This study provides evidence that Lasso (a splice variant of TEN2 lacking a 7-residue insert in
360 the β -propeller domain, TEN2-SS) functions specifically as an attractant for axons expressing
361 LPHN1, and proposes a molecular mechanism for this effect. By using microfluidic devices to
362 create long-term gradients of soluble proteins (Figure 3), we demonstrate that a gradient of
363 soluble ECD of Lasso can act as an attractant for axons from hippocampal neurons (Figs. 4, 5A-
364 E). Importantly, growing hippocampal neurons in a medium containing a uniform concentration of
365 Lasso had no effect on the length of their axons (Figure 5G). This shows that Lasso plays an
366 instructive role in the directionality, rather than the amount, of axonal growth. This is consistent
367 with the effect of other axon attractants acting via similar mechanisms. For example, short-term
368 exposure of axonal growth cones to gradients of BDNF stimulates IP₃-induced Ca²⁺ release (IICR)
369 that causes axonal attraction without an overall effect on neurite extension (Li et al., 2005).

370 One interesting observation from this project was the fasciculation of neurites in response to
371 soluble Lasso/TEN2 (Figure 5C, F). Fasciculation of axons is one of the major mechanisms of
372 axonal navigation, for example in limb development (Bastiani et al., 1986). While axonal
373 fasciculation has not been previously linked to a soluble ECD of TEN, neurite bundling was
374 actually observed in hippocampal cultures in response to TEN1 C-terminal peptide (TCAP-1) (Al
375 Chawaf et al., 2007). Furthermore, knockdown of TEN1 in *C. elegans* resulted in de-fasciculation
376 of the axons in the ventral nerve cord (Drabikowski et al., 2005). Potential mechanisms of axonal
377 bundling include actin reorganization induced by an LPHN1-mediated rise in cytosolic Ca²⁺, other
378 unknown interactions with cell adhesion molecules, or it could also be due to the divalent
379 Lasso/TEN2 fragment crosslinking adjacent axons, thus promoting their parallel elongation.

380 The soluble Lasso/TEN2 fragment could potentially have two membrane-anchored receptors: (i)
381 TEN2 itself, as a homophilic ligand (Bagutti et al., 2003; Rubin et al., 2002), or (ii) LPHN1, as a
382 heterophilic ligand (Boucard et al., 2014; Silva et al., 2011). However, we have not observed
383 TEN2 expression in growth cones of hippocampal axons (Figure 1E), but found it to be abundant
384 on dendrites (Silva et al., 2011) (Figure 1E, S1B). We also did not detect any appreciable binding
385 of the released Lasso ECD to membrane-anchored Lasso (Figure 2D, Figure 2—supplement 1,
386 B). In addition, homophilic interaction of Lasso/TEN2 actually has been reported to inhibit neurite
387 outgrowth in neuroblastoma cells (Beckmann et al., 2013), while we saw an opposite effect (Figs.
388 4, 5). Thus, the potential Lasso/TEN2 homophilic interaction could not explain the observed
389 axonal attraction. On the other hand, we found strong expression of LPHN1 on the axonal growth
390 cones of cultured hippocampal neurons (Figure 1E-I, S1C-F) (Silva et al., 2011). Importantly, the
391 released soluble ECD of Lasso strongly bound to LPHN1 that was expressed on neuroblastoma
392 cells or neuronal growth cones (Figure 2, Figure 2—supplements 1-2). Furthermore, we found
393 that deletion of LPHN1 precluded axonal attraction by Lasso (Figure 4), while it had no effect on
394 neuronal cell bodies and dendrites in the Somal Compartment. These data strongly implicate
395 LPHN1 in mediating Lasso-induced axon attraction.

396 Our studies also reveal the likely mechanism that underlies the Lasso/LPHN1-induced axonal
397 attraction. LPHN1 is a G-protein-coupled receptor (GPCR) that physically and functionally links
398 to $G\alpha_{q/11}$ (Rahman et al., 1999). Activation of LPHN1 by its non-pore-forming agonist, LTX^{N4C},
399 leads to aggregation of the NTF and CTF of LPHN1 (Silva et al., 2009; Volynski et al., 2004). This
400 results in assembly of a functional GPCR, with subsequent activation of the downstream signaling
401 cascade, which includes $G\alpha_{q/11}$, phospholipase C, production of IP₃ and IP₃-receptor-mediated
402 release of Ca²⁺ from intracellular stores (Capogna et al., 2003; Lajus et al., 2006; Volynski et al.,
403 2004), thus inducing IICR.

404 IICR is also regulated and enhanced by increased cAMP levels (Tojima et al., 2011), and we
405 previously demonstrated that activation of LPHN1 expressed in COS7 cells induces an increase
406 in cAMP production (Lelianova et al., 1997). In line with this, the recent study by Li et al. (2018)
407 confirmed the ability of LPHN1 to regulate cAMP signaling. In that work (Li et al., 2018), the cAMP
408 signaling interference system was based on HEK293 cells expressing exogenous β_2
409 adrenoceptor (β_2 AR). Activation of β_2 AR by its agonist led to an increase in cAMP production,
410 while a large excess of co-expressed LPHN1 interfered with β_2 AR signaling. This clearly suggests
411 that LPHN1 uses the same cAMP signaling machinery as β_2 AR, and that when LPHN1 is not
412 stimulated, it can titrate components of this machinery, decreasing their availability to β_2 AR.

413 In agreement with the role of Lasso as a functional LPHN1 agonist, the binding of the released
414 Lasso fragment to LPHN1 similarly causes the re-association of LPHN1 fragments (Figure 6) and
415 Ca^{2+} signaling (Figure 7A-C). A rise in cytosolic Ca^{2+} concentration, in turn, can increase the rate
416 of exocytosis, and we indeed observed enhanced acetylcholine release in mouse neuromuscular
417 junctions in response to soluble Lasso (Figure 7D-F). This response to Lasso was clearly
418 mediated by LPHN1, as it was not detected in neuromuscular preparations from LPHN1 KO mice
419 (Figure 7D-F). On the other hand, the effect of soluble Lasso on vesicular exocytosis was much
420 weaker – and probably more physiological – than the massive effect of LTX^{N4C}.

421 In addition to Ca^{2+} regulation, Lasso binding to LPHN1 can induce cAMP signaling. Indirect
422 evidence for this is provided by the cAMP signaling interference experiments mentioned above
423 (Li et al., 2018). When LPHN1 co-expressed with β_2 AR was stimulated for 24 hours with
424 Lasso/TEN2 (expressed on the same or opposite cells), this strongly decreased cAMP levels
425 induced by β_2 AR activation. The most likely reason could be that following an initial Lasso-
426 induced LPHN1 activation, which normally subsides within 30 min (Figure 7B), the continued
427 LPHN1 stimulation led to massive heterologous receptor desensitization (Kelly et al., 2008).

428 Intriguingly, the effects of soluble Lasso resemble the well-known mechanism that underpins
429 axonal attraction and consists of IP₃ receptor-mediated local release of Ca²⁺ from intracellular
430 stores, coupled with an increase in cAMP levels, that leads to increased exocytosis at the
431 advancing edge of a growth cone (Akiyama et al., 2009; Qu et al., 2002; Tojima et al., 2011;
432 Tojima and Kamiguchi, 2015). Thus, when a gradient of soluble Lasso ECD approaches one side
433 of an axonal growth cone, it may cause local activation of LPHN1 and its downstream signaling,
434 ultimately leading to IICR. Local IICR in growth cones can induce an increase in vesicular
435 exocytosis (as observed in our experiments with Lasso-G, Figure 7) and the remodeling of actin
436 filaments (Tojima et al., 2011). The resulting augmented membrane delivery and actin-driven
437 extension of filopodia at the edge facing a Lasso gradient would support the growth cone's
438 advance in this direction. Thus, based on all our data, we propose this chain of events
439 (summarized in Figure 8) as a likely mechanism for axonal attraction by soluble Lasso observed
440 in this study.

441 While TEN2 has been implicated in axon guidance in the visual pathway (Young et al., 2013),
442 here we report that it can also trigger axonal steering in developing hippocampal neurons, which
443 is consistent with the strong expression of both Lasso/TEN2 and LPHN1 in the hippocampus
444 (Davletov et al., 1998; Otaki and Firestein, 1999). Furthermore, both proteins are expressed
445 throughout the CNS, suggesting that this mechanism of soluble Lasso/LPHN1-mediated axonal
446 attraction may apply widely across the brain, especially in such areas as the cortex, cerebellum,
447 thalamus and spinal cord.

448 Interestingly, the splice variant of TEN2 (TEN2+SS), which contains the 7-amino acid insert in the
449 β-propeller domain and cannot mediate cell adhesion via LPHN1 (Li et al., 2018), might attract
450 dendrites instead of axons, in contrast to Lasso (TEN2-SS). Thus, in an artificial synapse
451 formation experiment (Li et al., 2018), HEK293 cells expressing TEN2+SS were seen covered by
452 neurites from co-cultured hippocampal neurons that contained GABA_A receptors. However, these

453 processes did not show a proportionate amount of PSD-95 and thus probably represented *en*
454 *passant* dendrites that were attracted to TEN2+SS cells, but unable to form mature inhibitory
455 synapses with them. This could be a mechanism by which TEN2+SS could provide a substrate
456 for the growth of dendrites searching for their ultimate target/s. Although the relative abundance
457 of Lasso and TEN2+SS in the brain is unknown, these data suggest that various TEN isoforms
458 could participate in distinct interactions, possibly with opposite results.

459 High expression of LPHN1 and Lasso/TEN2 throughout the CNS, combined with their
460 fundamental role in axon guidance, is consistent with lethal phenotypes observed in simpler
461 organisms (Langenhan et al., 2009; Mosca et al., 2012). In knockout mice, however, the
462 phenotype is less severe (Tobaben et al., 2002; Young et al., 2013) (Ushkaryov, to be published
463 elsewhere) suggesting that LPHN1 deletion is not completely penetrant, likely due to a
464 compensatory effect of multiple LPHN and TEN homologs expressed in the mammalian brain.
465 Indeed, LPHN1 can also weakly interact with TEN4 (Boucard et al., 2014), and LPHN3 can
466 interact with TEN1 (O'Sullivan et al., 2014). Moreover, LPHN and TEN isoform expression
467 patterns overlap (Oohashi et al., 1999; Sugita et al., 1998; Zhou et al., 2003). This predisposition
468 to compensation further raises the possibility that the mechanism of axonal guidance involving
469 the interaction of soluble TEN2 with LPHN1, described in this study, may occur between different
470 members of the LPHN and TEN families. These observations provide evidence of further diversity
471 of interactions and local specificity of developmental pathways for more accurate and plastic
472 patterning of neural networks within the mammalian CNS.

473 **MATERIALS AND METHODS**

474 **Key resources table**

Reagent type (species) or resource	Designation	Source or Reference	Identifiers	Additional information
Antibody	Anti-FLAG M2 affinity gel	Sigma-Aldrich	A2220	
Antibody	Chicken anti-myc	Millipore	AB3252 RRID:AB_2235702	(Immunocytochemistry 1:1,000)
Antibody	Mouse anti-actinin	Sigma-Aldrich	A7811	(Western blot 1:1,500)
Antibody	Mouse anti-FLAG M2	Sigma-Aldrich	F3165 RRID:AB_259529	(Immunocytochemistry 1:1,000)
Antibody	Mouse anti-Lasso/teneurin-2 C-terminus	(Silva et al., 2011)	dmAb	TN2C (Immunocytochemistry 1:300; Western blot 1:1,000)
Antibody	Mouse anti-MAP-2	Neuromics	MO22116	(Immunocytochemistry 1:1,000)
Antibody	Mouse anti-synapsin	Santa-Cruz Biotechnology	sc-376623 RRID:AB_11150313	(Immunocytochemistry 1:1,000)
Antibody	Mouse monoclonal anti-myc	Millipore	05-419 RRID:AB_309725	clone 9E10 (Immunocytochemistry 1:1000; Western blot 1:)
Antibody	Mouse monoclonal anti-V5	AbD Serotec/Bio-Rad	MCA1360	clone SV5-Pk1 (Immunocytochemistry 1:2,000)
Antibody	Rabbit anti-GFP	Thermo Fisher Scientific	A-11122 RRID: AB_221569	(Immunocytochemistry 1:1,000)
Antibody	Rabbit anti-NF-H	Neuromics	RA22116	(Immunocytochemistry 1:1,000; Western blot 1:10,000)
Antibody	Rabbit anti-PSD-95	Millipore	AB9708 RRID:AB_11212529	(Immunocytochemistry 1:2,000)
Antibody	Rabbit anti-Tau	Synaptic Systems	314 002 RRID:AB_993042	(Immunocytochemistry 1:1,000)
Antibody	Rabbit anti-V5	Thermo Fisher Scientific	PA1-29324 RRID:AB_1961277	(Immunocytochemistry 1:2,000)
Antibody	Rabbit polyclonal anti-LPHN1 NTF	(Davletov et al., 1998)	RL1	(Immunocytochemistry 1:1,000)
Antibody	Rabbit polyclonal anti-LPHN1-peptide	(Davydov et al., 2009)	PAL1	(Immunocytochemistry; Western blot 3 ng/mL)
Antibody	Sheep anti-teneurin-2 N-terminus	R&D systems	AF4578 RRID:AB_10719438	TN2N (Western blot 1 µg/mL)
Cell line (<i>Homo sapiens</i>)	HEK293A	ECCC	RRID:CVCL_6910	
Cell line (<i>Mus musculus</i>)	Neuroblastoma 2a	ATCC	RRID:CVCL_0470	
Chemical compound	B27 Supplement	Life Technologies	17504044	

Chemical compound	Ca-free Hibernate-A medium	BrainBits UK	HE-Ca	
Chemical compound	Fluo-4 acetomethoxy ester	Thermo Fisher Scientific	F14201	
Chemical compound	Insulin Transferrin Selenium Supplement	Life Technologies	41400045	
Chemical compound	Neurobasal-A medium	Thermo Fisher Scientific	21103049	
Chemical compound	Purified protein: BSA-TRITC	Thermo Fisher Scientific	A23016	
Chemical compound	Vybrant DiO	Thermo Fisher Scientific	V22886	
Commercial assay or kit	Amaxa Rat Neuron Nucleofector Kit	Lonza	VAPG-1003	
Commercial assay or kit	SuperSignal West Femto Maximum Sensitivity Substrate	Thermo Fisher Scientific	34094	
Other	Microfluidic Axon Isolation Devices (MAIDs)	Xona Microfluidics	SND150	
Recombinant DNA reagent	BLOCK-iT Lentiviral Pol II miR RNAi Expression System pLenti6/V5-GW/EmGFP-miR	Life Technologies	K4938-00	
Recombinant DNA reagent	Bottom pre-miRNA oligo targeting LPHN1 mRNA	This paper	LPHN1miR14B	Sequence provided under Methods
Recombinant DNA reagent	Lasso-A	(Silva et al., 2011)	GenBank: JF784341	
Recombinant DNA reagent	Lasso-D	(Silva et al., 2011)	GenBank: JF784344	
Recombinant DNA reagent	Lasso-FS	(Silva et al., 2011)	GenBank: JF784340	
Recombinant DNA reagent	Lasso-G	(Silva et al., 2011)	GenBank: JF784347	GST-Lasso
Recombinant DNA reagent	LPH-42	(Volynski et al., 2004)	GenBank:MF966512	V5-LPH-A
Recombinant DNA reagent	pLenti6.2-GW/EmGFP-miR negative control	Thermo Fisher Scientific	K4938-00	
Recombinant DNA reagent	Primer: N255: Neo Forward	This paper		Sequence provided under Methods
Recombinant DNA reagent	Primer: N424: Neo/LPHN1 Reverse	This paper		Sequence provided under Methods
Recombinant DNA reagent	Primer: N425: LPHN1 Forward	This paper		Sequence provided under Methods
Recombinant DNA reagent	Top pre-miRNA oligo targeting LPHN1 mRNA	This paper	LPHN1miR14T	Sequence provided under Methods
Peptide, recombinant protein	Purified protein: Alexa Fluor 647-labeled LTX ^{N4C}	(Volynski et al., 2004)	N/A	

Peptide, recombinant protein	Purified protein: Human BDNF	R&D Systems	248-BD	
Peptide, recombinant protein	Purified protein: Lasso-D	(Silva et al., 2011)	N/A	
Peptide, recombinant protein	Purified protein: Lasso-G	(Silva et al., 2011)	N/A	GST-Lasso
Peptide, recombinant protein	Purified protein: LTX ^{N4C}	(Volynski et al., 2003)	N/A	
Software	AxoScope 10	Axon Instruments		
Software	FIJI, ImageJ	NIMH, Bethesda, Maryland, USA	RRID:SCR_002285 RRID:SCR_003070	
Software	LSM 510 Software (for image acquisition)	Carl Zeiss Microimaging GmbH	LSM 510	
Software	LSM Image Browser (for image archiving and measurements)	Carl Zeiss Microimaging GmbH	RRID:SCR_014344	
Software	MATLAB	Mathworks	RRID:SCR_001622	
Software	MiniAnalysis	Synaptosoft		
Software	Volocity (for image acquisition and stitching)	Perkin-Elmer	RRID:SCR_002668	
Strain (<i>Escherichia coli</i>)	<i>E. coli</i> : K12 JM109	Promega Corporation	L2005	
Strain (<i>Mus musculus</i>)	Mouse: C57BL/6J, <i>Adgr1</i> ^{-/-} , LPHN1 KO	This paper	AG148/2	P0 hippocampus
Strain (<i>Mus musculus</i>)	Mouse: C57BL/6J, <i>Adgr1</i> ^{-/-} , LPHN1 KO	This paper	AG148/2	P21 <i>flexor digitorum brevis</i> muscle
Strain (<i>Rattus norvegicus</i>)	Rat: E18 hippocampus	BrainBits UK	Rhp	

475 **Chemical reagents**

476 All chemicals and reagents were purchased from Sigma-Aldrich, unless otherwise stated. Cell
477 culture reagents were from PAA Laboratories or Thermo Fisher Scientific. Purified proteins:
478 LTX^{N4C} (Volynski et al., 2003); LTX^{N4C} labeled with Alexa Fluor 647 (Volynski et al., 2004); Lasso-
479 G (Silva et al., 2011); Lasso-D (Silva et al., 2011) (all prepared in this laboratory); human BDNF
480 (R&D Systems, 248-BD); BSA-TRITC (Thermo Fisher Scientific, A23016).

481 **Antibodies**

482 The following antibodies were used in this work: Rabbit anti-NF-H (Neuromics, RA22116); mouse
483 anti-MAP-2 (Neuromics, MO22116); mouse monoclonal anti-V5 (clone SV5-Pk1, AbD
484 Serotec/Bio-Rad, MCA1360); rabbit anti-V5 (Thermo Fisher Scientific, PA1-29324;
485 RRID:AB_1961277); mouse monoclonal anti-myc (clone 9E10, Millipore, 05-419;
486 RRID:AB_309725); chicken anti-myc (Millipore, AB3252; RRID:AB_2235702); mouse anti-FLAG
487 M2 (Sigma-Aldrich, F3165; RRID:AB_259529); anti-FLAG M2 affinity gel (Sigma-Aldrich, A2220);
488 mouse anti-actinin (Sigma-Aldrich, A7811); rabbit polyclonal anti-LPHN1-peptide (PAL1,
489 (Davydov et al., 2009); rabbit polyclonal anti-LPHN1 NTF (RL1) (Davletov et al., 1998); mouse
490 anti-Lasso/TEN2 C-terminus (TN2C, dmAb) (Silva et al., 2011); sheep anti-TEN2 N-terminus
491 (TN2N, R&D systems, AF4578; RRID:AB_10719438); mouse anti-synapsin (Santa-Cruz
492 Biotechnology, sc-376623; RRID:AB_11150313); rabbit anti-PSD-95 (Millipore, AB9708;
493 RRID:AB_11212529); rabbit anti-Tau (Synaptic Systems, 314 002; RRID:AB_993042); rabbit
494 anti-GFP (Thermo Fisher Scientific, A-11122; RRID: AB_221569).

495 **Cell lines**

496 The following cell lines were used: human embryonic kidney cells (HEK293A, purchased from
497 ECCC; RRID:CVCL_6910); mouse neuroblastoma cells (NB2a, a kind gift from Dr. C. Isaac,
498 Imperial College London; originally from ATCC and subsequently authenticated by ATCC using
499 their proprietary methods.; RRID:CVCL_0470). Both cultures are mycoplasma-free, based on a
500 mycoplasma test kit Plasmotest (Invivogen).

501 **Animals and biological samples**

502 A LPHN1 KO mouse (strain AG148-2, *Adgr11*^{-/-}) was generated on the 129SvJ genetic
503 background. Briefly (details to be published elsewhere), the LPHN1 gene was isolated from a
504 BAC clone containing a 36-kbp fragment of mouse genomic DNA. This was used to design a

505 transfer vector for homologous recombination, containing a 13-kbp gene fragment of the LPHN1
506 gene, in which the intron between exons 1 and 2 was replaced with a neomycin gene/promoter
507 cassette flanked by two loxP sequences. This insert disrupted the open reading frame in the
508 mRNA transcribed from the resulting mutated LPHN1 gene. The transfer vector, carrying also a
509 negative selection marker (diphtheria toxin A-chain), was used to generate stably transfected
510 129Sv/J ES cell lines and chimeric mice, using standard transgenic techniques. Mice transmitting
511 the inactivated LPHN1 gene through the germline were selected, inbred, back-crossed onto
512 C57BL/6J background, and maintained at Charles River UK. LPHN1 gene disruption was
513 confirmed by Southern blotting, PCR amplification using multiple primer pairs and Western
514 blotting. The genotype of all animals used for breeding and tissue extraction was determined by
515 PCR. All procedures (breeding and Schedule 1) were approved by the University of Kent Animal
516 Welfare Committee and performed in accordance with Home Office regulations and the European
517 Convention for the Protection of Vertebrate Animals used for Experimental and Other Scientific
518 Purposes.

519 E18 hippocampi were obtained from rats (BrainBits UK, Rhp). P0 hippocampi were prepared from
520 P0 mice (strains: C57BL/6J, *Adgr11*^{+/+}, LPHN1 WT or AG148/2, *Adgr11*^{-/-}, LPHN1 KO). *Flexor*
521 *digitorum brevis* muscle preparations were isolated from P21 male mice (C57BL/6J or AG148/2).

522 **Molecular biology reagents**

523 The sequences of human Lasso (Ten-2) mutants used in this study are available at GenBank:
524 Lasso-FS (JF784340), Lasso-A (JF784341), Lasso-D (JF784344), GST-Lasso (JF784347). N-
525 and C-terminally tagged rat LPHN1 (termed also LPH-42, MF966512) was described previously
526 as V5-LPH-A (Volynski et al., 2004). All cDNAs were subcloned into the pcDNA3.1 vector
527 (Thermo Fisher Scientific). A negative control plasmid, pLenti6.2-GW/EmGFP-miR (Thermo
528 Fisher Scientific, K4938-00), was used for GFP expression, and the miRNA oligonucleotides listed
529 below were cloned into this vector for LPHN1 knock-down experiments.

530 Oligonucleotides for targeting LPHN1 mRNA were: LPHN1miR14T, (TGCTGATAAAC
531 AGAGCGCAGCACATAGTTTTGGCCACTGACTGACTATGTGCTGCTCTGTTTAT) and
532 LPHN1miR14B (CCTGATAAACAGAGCAGCACATAGTCAGTCAGTGGCCAAACTATGTGCT
533 GCGCTCTGTTTATC). PCR primers for genotype analysis were: Neo Forward (N255,
534 CGAGACTAGTGAGACGTGCTACTTCCATTTGTC); LPHN1 Forward (N425, CTGACCCATA
535 ACCTCCAAGATGATGTTTAC); Neo/LPHN1 Reverse (N424, GATCTTGTC
536 TCTGTGCGCCCGTA).

537 **Generation of stable cell lines**

538 Human embryonic kidney (HEK293A) and rat neuroblastoma (NB2a) cell lines were cultured
539 using standard techniques in DMEM with 10% heat-inactivated fetal bovine serum (FBS, PAA
540 Laboratories), at 5% CO₂ and 37 °C. Stable cell lines were generated using the Escort III
541 transfection reagent and Geneticin selection (Thermo Fisher Scientific). The positive cells were
542 further enriched by fluorescence-assisted cell sorting (BD Biosciences). All NB2a cell cultures
543 contain proliferating, spindle-like cells and differentiated, neuron-like cells. We have not observed
544 any difference in Lasso or LPHN1 expression between these two types of cell in stably transfected
545 NB2a cultures.

546 **Protein purification**

547 For increased expression of Lasso or LPH constructs, the complete medium was replaced with a
548 serum-free DMEM (for HEK23A cells) or Neurobasal-A containing supplements (for NB2a cells).
549 Lasso-D was purified by immunoaffinity chromatography. Briefly, serum-free medium conditioned
550 by HEK293A cells expressing Lasso-D was filtered through 0.2 µm filters and incubated with anti-
551 FLAG M2 affinity gel overnight at 4 °C. Lasso-D was then eluted with 20 mM triethylamine,
552 neutralized with 1 M HEPES, dialyzed against PBS, sterile-filtered for use in cell culture and

553 concentrated on sterile 30 kDa MWCO filtration units (Vivaspin, GE Lifesciences). Medium above
554 non-transfected cells was processed in the same manner and used as a negative control. Amount
555 and purity of concentrated Lasso-D were assessed by SDS-PAGE and Coomassie staining.
556 Activity was confirmed by measuring its binding to cell-surface or soluble LPHN1 constructs (Silva
557 et al., 2011).

558 **Primary neuronal cultures**

559 Hippocampal cultures were prepared from Sprague-Dawley E18 rat hippocampi (BrainBits UK),
560 according to the supplier's instructions, or dissected from P0 AG148/2 mouse pups (*Adgr11^{-/-}*,
561 LPH1 KO) under sterile conditions. Hippocampi were digested with 2 mg/ml papain in Ca²⁺-free
562 Hibernate-A medium and dissociated in Hibernate-A medium with B27 supplement using fire-
563 polished Pasteur pipettes. Cells were seeded in Neurobasal-A/B27 medium on poly-D-lysine-
564 coated 13-mm coverslips at 5 x 10⁴ cells/coverslip and maintained at 5 % CO₂ and 37 °C. The
565 medium was partially replaced at least once a week.

566 **Electroporation of neurons**

567 Primary hippocampal neurons were transfected using Amaxa Rat Neuron Nucleofector Kit
568 (Lonza) as described by the manufacturer. Briefly, dissociated cells were resuspended in Rat
569 Neuron Nucleofector Solution with Supplement, then mixed with 3 µg of pcDNA6-GFP and
570 electroporated in Nucleofector using the G-013 program. The transfected cells were resuspended
571 in 500 µl of a recovery medium, containing a 1:3 mixture of Hibernate-A/B27 and Ca-free
572 Hibernate-A (BrainBits UK), and incubated at 37 °C for 15 min. Cells were plated at a higher
573 concentration to compensate for cell death. Next day, 0.8 nM Lasso-D was added to the medium
574 (PBS was added to control medium). At 4 DIV, the cultured hippocampal cells were fixed with 4%
575 paraformaldehyde (PFA), stained and visualized as described below in Image Analysis.

576 **Cultures in MAIDs**

577 To investigate axonal responses to chemoattractant gradients, MAIDs (Figure 5) with 150 μm
578 separation walls (Xona Microfluidics LLC) were prepared in accordance with the manufacturer's
579 guidelines (Harris et al., 2007a; Harris et al., 2007b). Briefly, MAIDs were sterilized with ethanol,
580 washed with sterile water and dried. To facilitate firm attachment of MAIDs, 22 x 22 mm coverslips
581 (VWR International) were sonicated in water and ethanol, autoclaved, dried, then coated with 1
582 mg/ml poly-D-lysine overnight, washed, and dried overnight before the assembly.

583 For neuronal cell culture in MAIDs, E18 rat hippocampi were dissociated as above. Neurons (1.5
584 $\times 10^5/10 \mu\text{l}$) were added to Somal Compartments and allowed to settle for 30 min. MAIDs were
585 then filled with Neurobasal-A/B27. After 3 DIV, the medium in Axonal Compartments was carefully
586 replaced with medium containing soluble Lasso-D or with control medium. Alternatively,
587 HEK293A cells stably expressing Lasso-D (or untransfected) were plated in the wells of Axonal
588 Compartment. At 8 DIV, the cells were fixed and processed as described below.

589 **Protein diffusion in MAIDs**

590 For diffusion modeling experiments, MAIDs were assembled as above and filled with PBS; then
591 0.1 mg/ml BSA-TRITC (Thermo Fisher Scientific) in PBS was added to Axonal Compartments
592 without changing liquid level in any compartment (to avoid creating a hydrostatic pressure in the
593 microchannels). BSA-TRITC diffusion in MAIDs was monitored by time-lapse fluorescent imaging
594 of all compartments for 5 days under an Axiovert fluorescent microscope (Carl Zeiss) equipped
595 with a temperature- and humidity-controlling enclosure, and a Canon G5 camera. Fluorescence
596 intensity profiles across the microchannels at multiple time points were generated in ImageJ
597 (NIMH, Bethesda; RRID:SCR_002285, RRID:SCR_003070) and normalized to the fluorescence
598 profile of 100 ng/ml BSA-TRITC forced into the microchannels and both compartments.

599 **Immunocytochemistry**

600 Cells on coverslips or inside MAIDs were fixed for 10 min with 4% PFA (for staining requiring SDS
601 treatment to aid epitope retrieval, the fixative also included 0.1 % glutaraldehyde). Cells were
602 permeabilized with 0.1 % Triton X-100 (or 1% SDS for PAL1 and dmAb staining), washed, then
603 blocked for 1 h with 10 % goat serum in PBS and incubated with primary antibodies in blocking
604 solution (dilutions used were: PAL1, 3 ng/ml; dmAb, 1:300; anti-NF-H, anti-myc mAb, and anti-
605 GFP, 1:1,000; anti-V5, 1:2,000) for 1 h at room temperature (or overnight at 4 °C with PAL1 and
606 dmAb). The coverslips or MAIDs were then washed 3 times and incubated for 1 h with secondary
607 antibodies in blocking solution, followed by 3 washes. Coverslips were mounted using FluorSave
608 mounting medium (Calbiochem), while neurons in MAIDs were imaged within 4 hours after the
609 washes.

610 **Receptor patching**

611 NB2a cells stably expressing LPH-42 were grown on poly-D-lysine-coated coverslips in DMEM,
612 10 % fetal calf serum (PAA Laboratories) to 30–50% confluency and to test receptor clumping
613 incubated at 0 °C for 20 min in PBS with one of the 3 potential LPHN1 ligands: (1) 20 nM Lasso-
614 D, (2) 2 nM Alexa Fluor 647-labeled LTX^{N4C} (Volynski et al., 2004), or (3) rabbit anti-NTF
615 antibodies (RL1), followed by a 20-min incubation with Alexa Fluor 546-conjugated goat anti-
616 rabbit IgG. In control, only the fluorescent secondary antibody was added for the last 20 min. The
617 cells were then fixed for 10 min with 4 % PFA in PBS, blocked with 10 % goat serum in PBS, and
618 subsequent procedures were designed to reveal the distribution of the three components of each
619 assay (NTF, CTF, and ligand). First, in all experiments, the V5 epitope on LPHN1 NTF was
620 detected with a rabbit anti-V5 antibody (1 h in blocking solution), followed by Alexa Fluor 488-
621 conjugated goat anti-rabbit IgG and fixation. Subsequent staining depended on the ligand used:
622 (1) Lasso-D was stained using a mouse anti-FLAG mAb and Alexa Fluor 546-conjugated goat

623 anti-mouse IgG. For LPHN1 CTF detection, the cells were then permeabilized with 0.1 % Triton
624 X-100, incubated with a chicken anti-myc antibody, fixed, blocked, and stained with Alexa Fluor
625 647-conjugated anti-chicken antibody. (2) With LTX^{N4C}-induced patching, the cells were
626 permeabilized, incubated with a mouse anti-myc mAb, fixed, blocked, and stained with an Alexa
627 Fluor 546-conjugated anti-mouse IgG. (3) With RL1-induced patching (and in controls), the cells
628 were permeabilized, incubated with the chicken anti-myc antibody, fixed, blocked, and stained
629 with Alexa Fluor 647-conjugated anti-chicken antibody. The primary antibodies were used at
630 1:1000 dilution; the secondary antibodies, 1:2000; the cells were washed 3 times with PBS after
631 each stage. At the end, the cells were briefly fixed, blocked, washed, and mounted using
632 FluorSave reagent (Calbiochem, Cat. No. 345789).

633 **Image acquisition**

634 Images of axons in MAIDs were acquired on an Axiovert 200M microscope (Carl Zeiss) using LD
635 Plan-Neofluar 20x objective and Volocity-controlled camera, filters, shutter, and stage. Images
636 were taken with a 5 % overlap to facilitate stitching (Perkin-Elmer; RRID:SCR_002668). Blank
637 images were subtracted to correct for optical artifacts. The images were stitched automatically
638 and “despeckled”, using a 3x3 median filter (ImageJ). To correct for large illumination artifacts,
639 background was subtracted in ImageJ using the “Subtract background” plug-in, with a 100- μ m
640 window and the sliding paraboloid algorithm.

641 Images of immunostained cells and neurons on coverslips (other than for neurite tracing) were
642 acquired using an upright laser-scanning confocal microscope (LSM-510, Zeiss;
643 RRID:SCR_014344) equipped with 40x or 100x oil-immersion objectives; 488, 543, and 633 nm
644 lasers; and 505–530, 560–615, and >650 nm emission filters. Images for neurite tracing were
645 acquired using Axio Observer.Z1 microscope (Zeiss) equipped with Hamamatsu ORCA-Flash 4
646 sCMOS camera, EC Plan-Neofluar 40x objective, Colibri 2 LED illumination and appropriate

647 filters.

648 **Image analysis**

649 To correlate the polarity of LPH1 expression and growth cone turning, GFP images of growth
650 cones and preceding axons were traced using CorelTRACE X3 (Corel, Canada). The obtained
651 contour images were aligned along their median line, with all axons starting at the same point.
652 The images were then flipped so that the higher LPHN1 staining was located in the right half of
653 each growth cone. The trajectory of respective axons was then assessed: correlation was
654 considered positive if the axon approached its cone from the right quadrant. To plot Jeffreys
655 confidence intervals (CI) for a binomial distribution the standard formula was used: $CI =$
656 $p+z*\sqrt{p*(1-p)/n}$, where $z = 3$ for confidence level $CI = 0.9973$.

657 For profiling of neurite growth within MAID Axonal Compartments, regions of interest
658 encompassing the depth of the compartments, were selected, avoiding artefacts (e.g. antibody
659 aggregates or HEK cell bodies). The average fluorescence was determined as a function of
660 distance (see Fig 5A) from the separation wall and binned over 100 μm intervals. Background
661 fluorescence in the areas beyond 1200 μm from the wall (that contained no axons) was subtracted
662 from all other fluorescence values, and the results were used for statistical analysis as described
663 below.

664 For axon fasciculation measurements in MAIDs, the width of each axon/bundle was determined
665 in pixels at 100 μm from the separation wall and converted to μm .

666 Neurite tracing of GFP-positive neurons was performed in ImageJ (Schindelin et al., 2012) using
667 default settings in Simple Neurite Tracer plug-in (Longair et al., 2011). The longest neurite for
668 each cell was used as a single independent measurement (data obtained from three independent
669 cultures).

670 Analysis of the co-localization of the NTF, CTF, and respective ligands in the plasma membrane
671 was carried out using a method previously developed and tested (Silva et al., 2011). Here, the
672 confocal images were obtained near the middle of each cell (optical plane, $Z = 0.5 \mu\text{m}$). For
673 consistency, the recorded images were assigned false colors according to the detected protein,
674 irrespective of the actual fluorescence wavelength used for detection. The fluorescence profiles
675 for each protein along the cell's perimeter were collected using ImageJ. Pearson's correlation
676 coefficient r was then calculated for the pairs of resulting profiles obtained from 4-7 independent
677 experiments.

678 In the representative images that were used in the Figures, the contrast and brightness were
679 enhanced in the same manner as in respective control images.

680 **Fluorometry**

681 For experiments with LPHN1 KO and WT/HET cultures in MAIDs, the membranes of cell bodies
682 and axons were labeled using $5 \mu\text{M}$ DiO (Vybrant® DiO, Life Technologies) in Neurobasal-A,
683 containing B-27 supplement and 0.005% Pluronic F-127 (Sigma-Aldrich), which had been passed
684 through a $0.2 \mu\text{m}$ filter. After 30 min incubation, the excess dye was carefully washed 2 times,
685 and the cell bodies (Somal Compartments) and axons (Axonal Compartments) were solubilized
686 in 1% Triton X-100 in PBS. The undiluted axonal and 10-fold diluted somal fractions were
687 analyzed in microtiter plates using a Fluoroskan Ascent Fluorometer (485 nm excitation, 505 nm
688 emission filters) (Thermo Fisher Scientific). In some experiments, $2 \mu\text{L}$ samples of lysates were
689 individually measured using a NanoDrop ND-3300 Fluorospectrometer (Thermo Fisher Scientific)
690 with the following settings: 470 nm Blue LED excitation, 500-700 nm emission spectrum,
691 quantified at 504 nm. The levels of fluorescence were proportional to the amount of axons/cells
692 bodies present in respective compartments.

693 **Western blotting**

694 For Western Blot analysis of conditioned media, these were passed through 0.2 µm low protein-
695 binding filters (PALL, USA). The cells on coverslips were lysed in ice-cold RIPA buffer (1 %
696 sodium deoxycholate, 0.1 % SDS, 1 % Triton X-100; 10 mM Tris-HCl, pH 8; 140 mM NaCl),
697 supplemented with protease inhibitors and 1 mM EDTA. To prepare samples for electrophoresis,
698 the cell lysates and media were incubated at 50 °C for 30 min with sample buffer containing 2%
699 SDS and 100 mM DTT. The samples were separated on standard SDS-containing polyacrylamide
700 gels, blotted onto polyvinylidene fluoride membrane (Immobilon-P, IPVH00010, Merck),
701 incubated with primary antibodies diluted in 2 % BSA for TN2N or 5% milk for all other antibodies
702 (dilutions used were: PAL1, 1:500; dmAb, 1:1,000; TN2N, 1 µg/ml; actinin, 1:1,500; NF-H,
703 1:10,000) and respective horseradish-peroxidase conjugated secondary antibodies. The stained
704 membranes were visualized by WestFemto chemiluminescent substrate kit (Thermo Fisher
705 Scientific) and LAS3000 gel/blot documentation system (FUJIFILM).

706 **Measurements of cytosolic Ca²⁺**

707 Cytosolic Ca²⁺ concentration was monitored using Fluo-4 Ca²⁺ indicator (the method was also
708 described in (Silva et al., 2009; Volynski et al., 2004). The stably transfected NB2a cells
709 expressing LPH-42 were pre-incubated in serum-free medium for 24 h in 30 mm dishes. Then the
710 cells were equilibrated for 20 min in physiological buffer (in mM: NaCl, 145; KCl, 5.6; glucose, 5.6;
711 MgCl₂, 1; EGTA, 0.2; HEPES, 15; pH 7.4; BSA, 0.5 mg/ml) containing 2.5 µM Fluo-4
712 acetomethoxy ester (Fluo-4-AM, Thermo Fisher Scientific) and 10% Pluronic F-127, washed and
713 further incubated for 20 min for dye de-esterification. LPHN1-expressing cells were identified by
714 staining with primary mouse anti-V5 mAb pre-labeled with Alexa Fluor 568 (Zenon, Thermo Fisher
715 Scientific). Images were acquired every 5 s under the LSM510 microscope using a 40x Achroplan
716 water-dipping objective, 488 nm laser and a 505–550 nm band-pass emission filter. The following

717 protocols were typically applied (the addition times and final concentrations of the additives are
718 indicated, see also Figure 7—figure supplement 1, A and B). *Protocol 1*: 0 min, baseline recording;
719 5 min, 1 nM LTX^{N4C}, 360 nM Lasso-D, or control buffer; 30 min, 2 mM Ca²⁺; 50 min, 1 nM wild-
720 type α-LTX; 55 min, end. *Protocol 2*: 0 min, 2 mM Ca²⁺, baseline recording; 5 min, 360 nM Lasso-
721 D or control buffer; 30 min, 1 nM LTX^{N4C}; 80 min, 1 nM α-LTX; 90 min, end. Ca²⁺ fluorescence of
722 individual positive cells was quantified using the LSM510 software and normalized between the
723 starting fluorescence and maximal fluorescence induced by α-LTX.

724 **Electrophysiology**

725 MEPPs were recorded from isolated neuromuscular preparations by method also used in
726 (Lelyanova et al., 2009). *Flexor digitorum brevis* muscles were extracted from male P21 mice
727 (C57BL/6J: *Adgr11*^{+/+} or *Adgr11*^{-/-}), cleaned from connective tissue, fixed using entomological pins
728 in Petri dishes pre-coated with Sylgard silicone polymer (Dow Corning), and incubated in
729 constantly oxygenated physiological buffer containing (in mM): NaCl, 137; KCl, 5; MgCl₂, 1;
730 EGTA, 0.2; glucose, 5.6; HEPES, 10; pH 7.5; tetrodotoxin (Latoxan), 0.001). Sharp electrodes
731 with tip diameter < 0.5 μm and 30-60 MOhm impedance were produced on a P-97 puller (Sutter)
732 from borosilicate glass filament capillaries (1.5 mm; World Precision Instruments) and filled with
733 5 M sodium acetate. Spontaneous presynaptic activity (based on MEPPs detection) was recorded
734 using a system consisting of an Axoclamp 2B pre-amplifier (Axon Instruments) in the current
735 clamp mode, a secondary differential amplifier with a high-frequency filter (LPF202A, Warner
736 Instruments), a HumBug harmonic frequency quencher (Quest Scientific), a Digidata 1322A
737 digitizer (Axon Instruments), and a microcomputer running AxoScope software (Axon
738 Instruments). The recorded traces were subsequently analyzed using MiniAnalysis software
739 (Synaptosoft Inc.).

740 **Quantification and statistical analysis**

741 The data shown are the means \pm SEM, unless otherwise stated. A Lilliefors test was applied to
742 all data sets to assess normality in data distribution. Statistical significance was then determined
743 using two-tailed heteroscedastic t-test, with Bonferroni correction in cases of multiple pair-wise
744 comparisons. For non-normally distributed data, a Mann-Whitney test was applied. The axonal
745 fluorescence curves obtained from image analysis in MAIDs were compared using n-way ANOVA
746 algorithm (MATLAB; RRID:SCR_001622), where n reflected the number of factors involved in an
747 assay (treatment type, distance from the separation wall and batch number). To test for correlation
748 in axonal fasciculation measurements, a Pearson correlation coefficient (R^2) and the p values (to
749 test the correlation hypothesis) were calculated using MATLAB. Jeffreys confidence intervals
750 were used to assess statistical significance of correlation between LPH1 enrichment and growth
751 cone turning direction. Differences were considered significant if $p < 0.05$. The specific p and n
752 values are indicated in corresponding figure legends or the following notation is used to denote
753 statistical significance: NS (non-significant), $p > 0.05$; *, $p < 0.05$; **, $p < 0.01$; ***, $p < 0.001$. The
754 investigators were blinded to the identity of samples during data collection and analysis in all
755 experiments involving LPHN1 KO.

756 **Data and software availability**

757 The quantification methods used in the custom scripts are described above. Further requests for
758 custom scripts and data used in this study should be directed to N.V.V.
759 (nickolai.vysokov@gmail.com).

760 **ACKNOWLEDGMENTS**

761 Supported by a Wellcome Trust Project Grant WT083199MF, a Biotechnology and Biological
762 Science Research Council Core Support Grant BBF0083091, and core funding from the

763 University of Kent School of Pharmacy (to Y.A.U.); and in part by the Russian Scientific
764 Foundation Grant 14-44-00051 and 16-19-10597 (to A.G.T.).

765 **COMPETING INTEREST**

766 Nickolai Vysokov is affiliated with BrainPatch Ltd. and has no other competing interests to declare.

767 John-Paul Silva is affiliated with UCB-Pharma and has no other competing interests to declare.

768 Jason Suckling is affiliated with Thomsons Online Benefits and has no other competing interests
769 to declare.

770 John Cassidy is affiliated with Arix Bioscience and has no other competing interests to declare.

771 Alexander Tonevitsky is affiliated with Scientific Research Center Bioclinicum and has no other
772 competing interests to declare.

773 The other authors declare that they have no competing commercial interests in relation to this
774 work.

775 **REFERENCES**

776 Akiyama, H., Matsu-ura, T., Mikoshiba, K., and Kamiguchi, H. (2009). Control of neuronal growth
777 cone navigation by asymmetric inositol 1,4,5-trisphosphate signals. *Sci Signal* 2: ra34.

778 Al Chawaf A., Xu, K., Tan, L., Vaccarino, F.J., Lovejoy, D.A., and Rotzinger, S. (2007).
779 Corticotropin-releasing factor (CRF)-induced behaviors are modulated by intravenous
780 administration of teneurin C-terminal associated peptide-1 (TCAP-1). *Peptides* 28: 1406-1415.

781 Antinucci, P., Nikolaou, N., Meyer, M.P., and Hindges, R. (2013). Teneurin-3 specifies
782 morphological and functional connectivity of retinal ganglion cells in the vertebrate visual system.
783 *Cell Rep* 5: 582-592.

784 Ashton, A.C., Volynski, K.E., Lelianova, V.G., Orlova, E.V., Van Renterghem, C., Canepari, M.,
785 Seagar, M., and Ushkaryov, Y.A. (2001). α -Latrotoxin, acting via two Ca^{2+} -dependent pathways,
786 triggers exocytosis of two pools of synaptic vesicles. *J Biol Chem* 276: 44695-44703.

787 Bagutti, C., Forro, G., Ferralli, J., Rubin, B., and Chiquet-Ehrismann, R. (2003). The intracellular
788 domain of teneurin-2 has a nuclear function and represses zic-1-mediated transcription. *J Cell*
789 *Sci* 116: 2957-2966.

790 Bastiani, M.J., du Luc, S., and Goodman, C.S. (1986). Guidance of neuronal growth cones in the
791 grasshopper embryo. I. Recognition of a specific axonal pathway by the pCC neuron. *J Neurosci*
792 6: 3518-3531.

793 Baumgartner, S., Martin, D., Hagios, C., and Chiquet-Ehrismann, R. (1994). *ten^m*, a *Drosophila*
794 gene related to tenascin, is a new pair-rule gene. *EMBO J* 13: 3728-3740.

795 Beckmann, J., Schubert, R., Chiquet-Ehrismann, R., and Muller, D.J. (2013). Deciphering
796 teneurin domains that facilitate cellular recognition, cell-cell adhesion, and neurite outgrowth
797 using atomic force microscopy-based single-cell force spectroscopy. *Nano Lett* 13: 2937-2946.

798 Boucard, A.A., Maxeiner, S., and Südhof, T.C. (2014). Latrophilins function as heterophilic cell-
799 adhesion molecules by binding to teneurins: regulation by alternative splicing. *J Biol Chem* 289:
800 387-402.

801 Capogna, M., Volynski, K.E., Emptage, N.J., and Ushkaryov, Y.A. (2003). The α -latrotoxin mutant
802 LTX^{N4C} enhances spontaneous and evoked transmitter release in CA3 pyramidal neurons. *J*
803 *Neurosci* 23: 4044-4053.

804 Chen, S.Y., and Cheng, H.J. (2009). Functions of axon guidance molecules in synapse formation.
805 *Curr Opin Neurobiol* 19: 471-478.

806 Davletov, B.A., Meunier, F.A., Ashton, A.C., Matsushita, H., Hirst, W.D., Lelianova, V.G., Wilkin,
807 G.P., Dolly, J.O., and Ushkaryov, Y.A. (1998). Vesicle exocytosis stimulated by α -latrotoxin is
808 mediated by latrophilin and requires both external and stored Ca²⁺. *EMBO J* 17: 3909-3920.

809 Davydov, I.I., Fidalgo, S., Khaustova, S.A., Lelyanova, V.G., Grebenyuk, E.S., Ushkaryov, Y.A.,
810 and Tonevitsky, A.G. (2009). Prediction of epitopes in closely related proteins using a new
811 algorithm. *Bull Exp Biol Med* 148: 869-873.

812 Deák, F., Liu, X., Khvochtev, M., Li, G., Kavalali, E.T., Sugita, S., and Südhof, T.C. α -Latrotoxin
813 stimulates a novel pathway of Ca²⁺-dependent synaptic exocytosis independent of the classical
814 synaptic fusion machinery. *J Neurosci* 29: 8639-8648.

815 Drabikowski, K., Trzebiatowska, A., and Chiquet-Ehrismann, R. (2005). *ten-1*, an essential gene
816 for germ cell development, epidermal morphogenesis, gonad migration, and neuronal pathfinding
817 in *Caenorhabditis elegans*. *Dev Biol* 282: 27-38.

818 Feng, K., Zhou, X.H., Oohashi, T., Morgelin, M., Lustig, A., Hirakawa, S., Ninomiya, Y., Engel, J.,
819 Rauch, U., and Fassler, R. (2002). All four members of the Ten-m/Odz family of transmembrane
820 proteins form dimers. *J Biol Chem* 277: 26128-26135.

821 Hamann, J., Aust, G., Arac, D., Engel, F.B., Formstone, C., Fredriksson, R., Hall, R.A., Harty,
822 B.L., Kirchhoff, C., Knapp, B., Krishnan, A., Liebscher, I., Lin, H.H., Martinelli, D.C., Monk, K.R.,

823 Peeters, M.C., Piao, X., Promel, S., Schoneberg, T., Schwartz, T.W., Singer, K., Stacey, M.,
824 Ushkaryov, Y.A., Vallon, M., Wolfrum, U., Wright, M.W., Xu, L., Langenhan, T., and Schioth, H.B.
825 (2015). International Union of Basic and Clinical Pharmacology. XCIV. Adhesion G protein-
826 coupled receptors. *Pharmacol Rev* 67: 338-367.

827 Harris, J., Lee, H., Tu, C.T., Cribbs, D., Cotman, C., and Jeon, N.L. (2007). Preparing e18 cortical
828 rat neurons for compartmentalization in a microfluidic device. *J Vis Exp* 305.

829 Harris, J., Lee, H., Vahidi, B., Tu, C., Cribbs, D., Jeon, N.L., and Cotman, C. (2007). Fabrication
830 of a microfluidic device for the compartmentalization of neuron soma and axons. *J Vis Exp* 261.

831 Hong, W., Mosca, T.J., and Luo, L. (2012). Teneurins instruct synaptic partner matching in an
832 olfactory map. *Nature* 484: 201-207.

833 Hor, H., Francescato, L., Bartesaghi, L., Ortega-Cubero, S., Kousi, M., Lorenzo-Betancor, O.,
834 Jimenez-Jimenez, F.J., Gironell, A., Clarimon, J., Drechsel, O., Agundez, J.A., Kenzelmann, B.D.,
835 Chiquet-Ehrismann, R., Lleo, A., Coria, F., Garcia-Martin, E., Alonso-Navarro, H., Marti, M.J.,
836 Kulisevsky, J., Hor, C.N., Ossowski, S., Chrast, R., Katsanis, N., Pastor, P., and Estivill, X. (2015).
837 Missense mutations in TENM4, a regulator of axon guidance and central myelination, cause
838 essential tremor. *Hum Mol Genet* 24: 5677-5686.

839 Ichtchenko, K., Bittner, M.A., Krasnoperov, V., Little, A.R., Chepurny, O., Holz, R.W., and
840 Petrenko, A.G. (1999). A novel ubiquitously expressed α -latrotoxin receptor is a member of the
841 CIRL family of G-protein-coupled receptors. *J Biol Chem* 274: 5491-5498.

842 Kaech, S., and Banker, G. (2006). Culturing hippocampal neurons. *Nat Protoc* 1: 2406-2415.

843 Karaulanov, E., Bottcher, R.T., Stannek, P., Wu, W., Rau, M., Ogata, S., Cho, K.W., and Niehrs,
844 C. (2009). Unc5B interacts with FLRT3 and Rnd1 to modulate cell adhesion in *Xenopus* embryos.
845 *PLoS One* 4: e5742.

846 Kelly, E., Bailey, C.P., and Henderson, G. (2008). Agonist-selective mechanisms of GPCR
847 desensitization. *Br J Pharmacol* 153 Suppl 1: S379-S388.

848 Lajus, S., Vacher, P., Huber, D., Dubois, M., Benassy, M.N., Ushkaryov, Y., and Lang, J. (2006).
849 α -Latrotoxin induces exocytosis by inhibition of voltage-dependent K⁺ channels and by stimulation
850 of L-type Ca²⁺ channels via latrophilin in β -cells. *J Biol Chem* 281: 5522-5531.

851 Langenhan, T., Promel, S., Mestek, L., Esmaeili, B., Waller-Evans, H., Hennig, C., Kohara, Y.,
852 Avery, L., Vakonakis, I., Schnabel, R., and Russ, A.P. (2009). Latrophilin signaling links anterior-
853 posterior tissue polarity and oriented cell divisions in the *C. elegans* embryo. *Dev Cell* 17: 494-
854 504.

855 Leamey, C.A., Merlin, S., Lattouf, P., Sawatari, A., Zhou, X., Demel, N., Glendining, K.A.,
856 Oohashi, T., Sur, M., and Fassler, R. (2007). Ten_m3 regulates eye-specific patterning in the
857 mammalian visual pathway and is required for binocular vision. *PLoS Biol* 5: e241.

858 Lelianova, V.G., Davletov, B.A., Sterling, A., Rahman, M.A., Grishin, E.V., Totty, N.F., and
859 Ushkaryov, Y.A. (1997). α -Latrotoxin receptor, latrophilin, is a novel member of the secretin family
860 of G protein-coupled receptors. *J Biol Chem* 272: 21504-21508.

861 Lelyanova, V.G., Thomson, D., Ribchester, R.R., Tonevitsky, A.G., and Ushkaryov, Y.A. (2009).
862 Activation of α -latrotoxin receptors in neuromuscular synapses leads to a prolonged splash
863 acetylcholine release. *Bull Exp Biol Med* 147: 701-703.

864 Levine, A., Bashan-Ahrend, A., Budai-Hadrian, O., Gartenberg, D., Menasherow, S., and Wides,
865 R. (1994). Odd Oz: a novel *Drosophila* pair rule gene. *Cell* 77: 587-598.

866 Li, J., Shalev-Benami, M., Sando, R., Jiang, X., Kibrom, A., Wang, J., Leon, K., Katanski, C.,
867 Nazarko, O., Lu, Y.C., Sudhof, T.C., Skiniotis, G., and Arac, D. (2018). Structural basis for
868 teneurin function in circuit-wiring: a toxin motif at the synapse. *Cell* 173: 735-748.

869 Li, Y., Jia, Y.C., Cui, K., Li, N., Zheng, Z.Y., Wang, Y.Z., and Yuan, X.B. (2005). Essential role of
870 TRPC channels in the guidance of nerve growth cones by brain-derived neurotrophic factor.
871 *Nature* 434: 894-898.

872 Longair, M.H., Baker, D.A., and Armstrong, J.D. (2011). Simple Neurite Tracer: open source
873 software for reconstruction, visualization and analysis of neuronal processes. *Bioinformatics* 27:
874 2453-2454.

875 Matsushita, H., Lelianaova, V.G., and Ushkaryov, Y.A. (1999). The latrophilin family: multiply
876 spliced G protein-coupled receptors with differential tissue distribution. *FEBS Lett* 443: 348-352.

877 Minet, A.D., Rubin, B.P., Tucker, R.P., Baumgartner, S., and Chiquet-Ehrismann, R. (1999).
878 Teneurin-1, a vertebrate homologue of the *Drosophila* pair-rule gene ten-m, is a neuronal protein
879 with a novel type of heparin-binding domain. *J Cell Sci* 112: 2019-2032.

880 Mosca, T.J., Hong, W., Dani, V.S., Favaloro, V., and Luo, L. (2012). Trans-synaptic Teneurin
881 signalling in neuromuscular synapse organization and target choice. *Nature* 484: 237-241.

882 O'Sullivan, M.L., Martini, F., von, D.S., Comoletti, D., and Ghosh, A. (2014). LPHN3, a presynaptic
883 adhesion-GPCR implicated in ADHD, regulates the strength of neocortical layer 2/3 synaptic input
884 to layer 5. *Neural Dev* 9: 7.

885 Oohashi, T., Zhou, X.H., Feng, K., Richter, B., Morgelin, M., Perez, M.T., Su, W.D., Chiquet-
886 Ehrismann, R., Rauch, U., and Fassler, R. (1999). Mouse Ten-m/Odz is a new family of dimeric
887 type II transmembrane proteins expressed in many tissues. *J Cell Biol* 145: 563-577.

888 Otaki, J.M., and Firestein, S. (1999). Neurestin: putative transmembrane molecule implicated in
889 neuronal development. *Dev Biol* 212: 165-181.

890 Qu, X., Wei, H., Zhai, Y., Que, H., Chen, Q., Tang, F., Wu, Y., Xing, G., Zhu, Y., Liu, S., Fan, M.,
891 and He, F. (2002). Identification, characterization, and functional study of the two novel human
892 members of the semaphorin gene family. *J Biol Chem* 277: 35574-35585.

893 Rahman, M.A., Ashton, A.C., Meunier, F.A., Davletov, B.A., Dolly, J.O., and Ushkaryov, Y.A.
894 (1999). Norepinephrine exocytosis stimulated by α -latrotoxin requires both external and stored
895 Ca^{2+} and is mediated by latrophilin, G proteins and phospholipase C. *Phil Trans R Soc Lond B*
896 354: 379-386.

897 Rubin, B.P., Tucker, R.P., Martin, D., and Chiquet-Ehrismann, R. (1999). Teneurins: a novel
898 family of neuronal cell surface proteins in vertebrates, homologous to the *Drosophila* pair-rule
899 gene product Ten-m. *Dev Biol* 216: 195-209.

900 Rubin, B.P., Tucker, R.P., Brown-Luedi, M., Martin, D., and Chiquet-Ehrismann, R. (2002).
901 Teneurin 2 is expressed by the neurons of the thalamofugal visual system *in situ* and promotes
902 homophilic cell-cell adhesion in vitro. *Development* 129: 4697-4705.

903 Schindelin, J., Arganda-Carreras, I., Frise, E., Kaynig, V., Longair, M., Pietzsch, T., Preibisch, S.,
904 Rueden, C., Saalfeld, S., Schmid, B., Tinevez, J.Y., White, D.J., Hartenstein, V., Eliceiri, K.,
905 Tomancak, P., and Cardona, A. (2012). Fiji: an open-source platform for biological-image
906 analysis. *Nat Methods* 9: 676-682.

907 Silva, J.P., Lelianova, V., Hopkins, C., Volynski, K.E., and Ushkaryov, Y. (2009). Functional cross-
908 interaction of the fragments produced by the cleavage of distinct adhesion G-protein-coupled
909 receptors. *J Biol Chem* 284: 6495-6506.

910 Silva, J.P., Lelianova, V.G., Ermolyuk, Y.S., Vysokov, N., Hitchen, P.G., Berninghausen, O.,
911 Rahman, M.A., Zangrandi, A., Fidalgo, S., Tonevitsky, A.G., Dell, A., Volynski, K.E., and
912 Ushkaryov, Y.A. (2011). Latrophilin 1 and its endogenous ligand Lasso/teneurin-2 form a high-
913 affinity transsynaptic receptor pair with signaling capabilities. *Proc Natl Acad Sci U S A* 108:
914 12113-12118.

915 Sollner, C., and Wright, G.J. (2009). A cell surface interaction network of neural leucine-rich
916 repeat receptors. *Genome Biol* 10: R99.

917 Sugita, S., Ichtchenko, K., Khvotchev, M., and Südhof, T.C. (1998). α -Latrotoxin receptor
918 CIRL/latrophilin 1 (CL1) defines an unusual family of ubiquitous G-protein-linked receptors. G-
919 protein coupling not required for triggering exocytosis. *J Biol Chem* 273: 32715-32724.

920 Suzuki, N., Mizuniwa, C., Ishii, K., Nakagawa, Y., Tsuji, K., Muneta, T., Sekiya, I., and Akazawa,
921 C. (2014). Teneurin-4, a transmembrane protein, is a novel regulator that suppresses
922 chondrogenic differentiation. *J Orthop Res* 32: 915-922.

923 Taylor, A.M., Blurton-Jones, M., Rhee, S.W., Cribbs, D.H., Cotman, C.W., and Jeon, N.L. (2005).
924 A microfluidic culture platform for CNS axonal injury, regeneration and transport. *Nat Methods* 2:
925 599-605.

926 Tobaben, S., Südhof, T.C., and Stahl, B. (2002). Genetic analysis of α -latrotoxin receptors reveals
927 functional interdependence of CIRL/Latrophilin 1 and neurexin I α . *J Biol Chem* 277: 6359-6365.

928 Tojima, T., Hines, J.H., Henley, J.R., and Kamiguchi, H. (2011). Second messengers and
929 membrane trafficking direct and organize growth cone steering. *Nat Rev Neurosci* 12: 191-203.

930 Tojima, T., and Kamiguchi, H. (2015). Exocytic and endocytic membrane trafficking in axon
931 development. *Dev Growth Differ* 57: 291-304.

932 Tucker, R.P., and Chiquet-Ehrismann, R. (2006). Teneurins: a conserved family of
933 transmembrane proteins involved in intercellular signaling during development. *Dev Biol* 290:
934 237-245.

935 Volynski, K.E., Capogna, M., Ashton, A.C., Thomson, D., Orlova, E.V., Manser, C.F., Ribchester,
936 R.R., and Ushkaryov, Y.A. (2003). Mutant α -latrotoxin (LTX^{N4C}) does not form pores and causes
937 secretion by receptor stimulation. This action does not require neuroligins. *J Biol Chem* 278: 31058-
938 31066.

939 Volynski, K.E., Silva, J.P., Lelianaova, V.G., Atiqur, R.M., Hopkins, C., and Ushkaryov, Y.A. (2004).
940 Latrophilin fragments behave as independent proteins that associate and signal on binding of
941 LTX^{N4C}. *EMBO J* 23: 4423-4433.

942 Vysokov, N.V., Silva, J.P., Lelianaova, V.G., Ho, C., Djamgoz, M.B., Tonevitsky, A.G., and
943 Ushkaryov, Y.A. (2016). The mechanism of regulated release of Lasso/teneurin-2. *Front Mol*
944 *Neurosci* 9: 59.

945 Young, T.R., Bourke, M., Zhou, X., Oohashi, T., Sawatari, A., Fassler, R., and Leamey, C.A.
946 (2013). Ten-m2 is required for the generation of binocular visual circuits. *J Neurosci* 33: 12490-
947 12509.

948 Zhou, X.H., Brandau, O., Feng, K., Oohashi, T., Ninomiya, Y., Rauch, U., and Fassler, R. (2003).
949 The murine Ten-m/Odz genes show distinct but overlapping expression patterns during
950 development and in adult brain. *Gene Expr Patterns* 3: 397-405.

951 Zicha, D., Dunn, G.A., and Brown, A.F. (1991). A new direct-viewing chemotaxis chamber. *J Cell*
952 *Sci* 99 (Pt 4): 769-775.

953

954

955 **FIGURE LEGENDS**

956 **Figure 1** with 1 supplement

957 **Lasso is cleaved and released into the medium during neuronal development. A.**

958 Recombinant Lasso constructs used in this work (FS, full size). The three proteolytic cleavage

959 sites and the SS splice site are indicated. The antibody recognition sites/epitopes are shown by

960 bars above the structure. Scale bar, 200 amino acids. **B.** Intracellular processing and release of

961 TENs. **Left**, TEN2 is constitutively cleaved in the trans-Golgi vesicles by furin at site 1. **Middle**,

962 when delivered to the cell surface, the ECD remains tethered to the membrane and functions as

963 a cell-surface receptor. **Right**, regulated cleavage at site 3 releases the ECD into the medium. **C.**

964 Expression of Lasso and release of its ECD fragment in hippocampal neurons in culture. Rat

965 hippocampal neurons were cultured for 3, 7 and 14 days, and proportionate amounts of the

966 conditioned media and cell lysates were separated by SDS-PAGE. A Western blot (representative

967 of three independent experiments, which all gave similar results) was stained for Lasso, LPHN1,

968 neurofilament-H (NF-H), and actinin. The doublet bands corresponding to splice variants of full-

969 size Lasso (FS) and the fragment of ECD (Frag.) cleaved at site 1 are indicated by arrowheads.

970 **D.** Quantification of Western blots (as in C), using Lasso C-terminus staining data. **E.** Axonal

971 growth cones (white arrowheads) do not express Lasso/teneurin-2. Neurons in a 9 DIV

972 hippocampal culture were permeabilized and stained for the axonal protein Tau (green) and Lasso

973 (TN2C, red) (representative image from $n = 5$ experiments). **F.** A detailed study of growth cones.

974 Hippocampal neurons were transfected with a vector encoding GFP, then, after 14 DIV, stained

975 for LPHN1 (PAL1 and Alexa 647-conjugated secondary antibody, magenta), and axonal growth

976 cones were visualized by GFP fluorescence (green). **G, H.** Correlation of LPHN1 polarization

977 within a growth cone with its recent travel trajectory. **G left**, a fluorescent image of a growth cone

978 stained for LPHN1 (magenta). **G right**, the same image in false color (contour based on GFP

979 staining), demonstrating LPHN1 polarization on the right side. **H left**, the contours of 13 roughly

980 symmetrical growth cones and their preceding axons were aligned to locate the stronger LPHN1
981 staining on the right. Note, that all axons approach growth cones from the right low quadrant. **H**
982 **right**, the proportion of right- and left-turning growth cones plotted with Jeffreys 99.73%
983 confidence intervals for a binomial parameter; ***, $p < 0.001$; $n = 13$. **I.** LPHN1 is found within
984 filopodia and lamellipodia on the leading edge (left, arrowheads), but not on the trailing edge
985 (right) of a growth cone. Green, GFP fluorescence; magenta, PAL1 staining for LPHN1.

986 **Figure 1–figure supplement 1**

987 **Lasso is expressed on dendrites and LPHN1 on axonal growth cones in developing**
988 **neurons.** **A.** Proportional expression of full-size Lasso and its fragments in hippocampal neurons
989 in culture. The data are from Western blots (as in Figure 1C, $n = 3$), stained using the TN2C
990 antibody. **B.** Lasso (red) is strongly expressed on dendritic shafts and dendritic growth cones
991 (black arrowhead). Neurons in 7-9 DIV hippocampal cultures were stained for Lasso/teneurin-2
992 using TN2C antibody. **C.** LPHN1 is expressed in axons and axonal growth cones (white arrow) in
993 cultured rat hippocampal neurons. 7-9 DIV neuronal cultures were permeabilized and stained for
994 LPHN1 (green) and synapsin (red). A growth cone is indicated by the white arrow. **D.** LPHN1 is
995 enriched in *en passant* synapses. A 9 DIV hippocampal culture was stained for Lasso (TN2C,
996 green) and postsynaptic structural protein, PSD-95 (red). Synapses are indicated by asterisks;
997 the growth cone, by a white arrowhead. **E.** Knockdown of LPHN1. Hippocampal neurons were
998 transfected with a bicistronic vector, encoding GFP and an shRNA against LPHN1, then at 14
999 DIV stained for LPHN1 (magenta) and imaged. Note that the growth cone of a knockdown neuron
1000 (green arrow) lacks LPHN1, while the growth cone of an uninfected neuron (arrowhead)
1001 expresses LPHN1. **F.** LPHN1 is expressed near the leading edge of turning growth cones. Left,
1002 GFP fluorescence of a growth cone. Right, the same growth cone stained for LPHN1 and
1003 rendered in false color. Note two peaks of LPHN1 quantity (red): in the central region (immediately
1004 above the “neck”, i.e. the end of axon shaft), and near the actively growing side of the growth

1005 cone. **G.** An average profile of LPHN1 expression within turning growth cones. LPHN1
1006 fluorescence was quantified along the median line of turning growth cones, expressed as % of
1007 maximal fluorescence and plotted against the normalized length of growth cones (distance
1008 expressed as %). The data are the mean values \pm SEM; $n = 9$. Note the bimodal distribution of
1009 LPHN1 expression.

1010

1011 **Figure 2** with 2 supplements

1012 **Soluble Lasso binds to LPHN1 on other cells. A.** A scheme of LPHN and Lasso constructs
1013 used in this experiment. LPH-82 is LPHN1 with the ECD from another adhesion G-protein-coupled
1014 receptor, EMR2, used as a negative control. **B.** Purification of Lasso-D. Lasso-D was expressed
1015 in stably transfected HEK293 cells, then purified on a column with anti-FLAG Ab and analyzed by
1016 SDS-PAGE in a 5% gel, stained with Coomassie R250. **C-E.** Interaction between the soluble
1017 Lasso species and NB2a cells expressing LPHN1, LPH-82, or Lasso-A. Cells expressing LPHN1
1018 (**C, panels 2, 3**), but not Lasso-A or Lasso-FS (**D**) or mutant LPH-82 (**C, panel 4**) are able to
1019 interact with Lasso-D or Lasso-A. **E, panel 1.** Short-term, high-density incubation of cells
1020 expressing LPHN1 and membrane-anchored Lasso-A allows these proteins to form inter-cellular
1021 contacts. **E, panel 2.** After a 48-h co-culture, a sufficient amount of Lasso-A is released into the
1022 medium, diffuses away from Lasso-A expressing cells (arrowhead) and can be detected
1023 interacting with distant LPHN1-expressing cells (arrow). Images are representative of $n = 6-7$
1024 independent experiments.

1025 **Figure 2—figure supplement 1**

1026 **Soluble Lasso specifically binds to LPHN1-expressing cells.** Interaction between the soluble
1027 Lasso species and NB2a cells expressing LPHN1 or Lasso-A. Cells expressing LPHN1 (**A**), but

1028 not Lasso-A (**B**), are able to bind the soluble Lasso-D. **C**. Binding of the soluble Lasso ECD
1029 released by the cells expressing the full-size Lasso-A to the surface of cells expressing LPHN1,
1030 after 48 h in co-culture. Note the lack of Lasso-D binding to cells not expressing LPHN1 (A-C)
1031 and the clumping of both proteins (C). Images are representative of $n = 7$ independent
1032 experiments.

1033 **Figure 2—figure supplement 2**

1034 **Soluble Lasso specifically binds to LPHN1 on axonal growth cones.** Hippocampal neurons
1035 from LPHN1 WT or KO newborn mice were grown in culture for 14 days and then incubated with
1036 the medium from NB2a cells stably expressing Lasso-D. The cultures were fixed and stained for
1037 LPHN1 (PAL1, green) and exogenous Lasso-D (FLAG, red). **A**. Two examples of LPHN1 WT
1038 axonal growth cones. **B**. An example of LPHN KO growth cones. Asterisks, axonal varicosities;
1039 arrowheads, axonal growth cones. The images are representative of 5-7 independent
1040 measurements, which all gave similar results. Note that LPHN1 KO neurons do not exhibit LPHN1
1041 staining (green), only showing autofluorescence, and do not appreciably bind Lasso-D (red). **C**.
1042 Quantification of the immunostaining data from $n = 3$ independent experiments. In control
1043 experiments, only secondary antibodies were used. Student's t-test with Bonferroni correction: *,
1044 $p = 0.031$; **, $p = 0.009$.

1045

1046 **Figure 3**

1047 **Using MAIDs to study axonal attraction by soluble chemoattractants.** **A**. Left, a photograph
1048 of a MAID. Center, a scheme of the experiment: neurons are seeded into the Somal Compartment
1049 and their neurites grow into the Axonal Compartment; both compartments are then stained for
1050 NF-H (axons) and MAP-2 (dendrites). Right, an enlarged portion of the separating wall showing

1051 the principles of fluorescence measurements in the Axonal Compartment. **B.** Fluorescent images
1052 from the same MAID stained for NF-H (green) and MAP-2 (red) showing that axons penetrate
1053 into the Axonal Compartment significantly more readily than dendrites. **C.** Profiles of NF-H and
1054 MAP-2 fluorescence in the Axonal Compartment, normalized to respective fluorescence in the
1055 Somal Compartment show that the relative degree of penetration of axons is ~5-fold higher
1056 compared to dendrites. **D.** Gradients of soluble proteins can be established within microchannels
1057 and maintained for several days. Top, a scheme of the experiment: TRITC-conjugated BSA was
1058 added to the Axonal Compartment and monitored using time-lapse fluorescent microscopy.
1059 Middle, fluorescence distribution 2 days after TRITC-BSA addition. Bottom, fluorescence
1060 distribution after filling the whole MAID with TRITC-BSA. **E.** Quantification of the TRITC-BSA
1061 gradient within microchannels (normalized to 100 $\mu\text{g/ml}$ TRITC-BSA). The mean values are
1062 shown \pm SEM; $n = 4$. **F-H.** A gradient of BDNF in MAIDs acts as an axonal attractant. **F.** A scheme
1063 of the experiment. **G.** Representative images of NF-H-positive axons in the Axonal Compartment
1064 exposed to control conditions (**left**) or to a BDNF gradient in the microchannels (**right**). **H. Left,**
1065 Average profiles of normalized NF-H fluorescence in the presence or absence of BDNF (2-way
1066 ANOVA: **, $p = 0.002$; $F_{1,84} = 10.15$). **Right,** integrated NF-H fluorescence between 0 and 500
1067 μm from the separating wall (t-test: *, $p = 0.04$; $n = 5$).

1068

1069 **Figure 4** with 1 supplement

1070 **A gradient of soluble Lasso-D induces axonal attraction via LPHN1.** **A.** A scheme of the
1071 experiment: hippocampal neurons were cultured in Somal Compartments, purified Lasso was
1072 added to Axonal Compartments at 3 DIV. **B.** Lasso remains intact in the Axonal Compartment.
1073 The media from Axonal Compartments were collected at 8 DIV and analyzed by Western blotting.
1074 **C.** Images of NF-H-positive axons in the Axonal Compartment exposed to control medium (left)

1075 or Lasso-D (right). **D.** Analysis of axonal growth in Axonal Compartments. **Left**, profiles of NF-H
1076 immunofluorescence with and without Lasso-D (3-way ANOVA: ***, $p < 0.001$; $F_{1,144} = 12.92$).
1077 **Right**, average integrated immunofluorescence at 0-500 μm from the wall, with and without
1078 Lasso-D (t-test: *, $p = 0.027$; $n = 7$). **E.** Knockout of LPHN1 blocks axonal attraction by soluble
1079 Lasso. Hippocampal neurons from *Adgrl1*^{-/-} (LPHN1 KO) and *Adgrl1*^{+/+} (LPHN1 WT) mice were
1080 cultured in MAIDs and exposed to Lasso-D gradient. The amount of cellular material in each
1081 compartment was quantified by DiO labeling at 8 DIV. **E. Left**, LPHN1 KO cultures sent
1082 significantly fewer neurites to Lasso-containing Axonal Compartments compared to WT cultures
1083 (t-test: ***, $p < 0.001$, $n = 3$). **Right**, there was no difference in the number of cells, dendrites and
1084 axons in the Somal Compartments between the two types of cultures (t-test: N.S., $p = 0.4$, $n = 3$).

1085 **Figure 4—figure supplement 1**

1086 **Knockout of LPHN1 prevents axonal attraction by soluble Lasso.** **A.** Experimental
1087 hypothesis: predicted behavior of LPHN1 KO axons in response to a gradient of soluble Lasso.
1088 **B.** Polymerase chain reaction (PCR)-based genotyping of 6 newborn pups from 3 mothers used
1089 to prepare hippocampal cultures in MAIDs. The PCR primers used and the sizes of amplified
1090 fragments are shown on the right; the deduced genotypes are indicated at the bottom.

1091

1092 **Figure 5**

1093 **A spatio-temporal gradient of soluble Lasso induces axonal attraction and fasciculation,**
1094 **but does not increase axonal length.** **A.** A scheme of the experiment: HEK293A cells stably
1095 transfected with Lasso-D were cultured in the wells of Axonal Compartments; untransfected cells
1096 were used as a control. **B.** A representative Western blot of the media from Axonal Compartments;
1097 Lasso-D is secreted by transfected HEK293A cells only and is stable. **C.** Images of NF-H-positive

1098 axons (green) and MAP-2-positive dendrites (red) in the Axonal Compartment exposed to
1099 temporal gradients formed by control cells (top) or Lasso-D-expressing cells (bottom). D. Left,
1100 profiles of axons in Axonal Compartments, identified by NF-H immunofluorescence, exposing a
1101 difference between control and Lasso-secreting cells (3-way ANOVA: **, $p = 0.006$; $n = 7$, $F_{1,84} =$
1102 7.89). Right, average integrated axonal fluorescence at 0-500 μm from the wall, with control or
1103 Lasso-secreting cells (t-test: *, $p = 0.045$; $n = 7$). E. Left, profiles of dendrites in Axonal
1104 Compartments, identified by MAP-2 immunofluorescence, with control or Lasso-secreting cells
1105 (3-way ANOVA: non-significant, $p = 0.23$; $F_{1,84} = 1.46$). Right, average integrated dendritic
1106 fluorescence at 0-500 μm from the wall, with control or Lasso-secreting cells (t-test: non-
1107 significant, $p = 0.54$; $n = 7$). F. Soluble released Lasso-D induces axonal fasciculation. The width
1108 of all NF-H-positive axonal bundles was measured at 100 μm from the separating wall. The
1109 degree of fasciculation correlates with Lasso concentration (Pearson's correlation: $R^2 = 0.43$, $p =$
1110 0.041). G. Soluble Lasso has no effect on axon length in cultured hippocampal cells. Left.
1111 Representative images of GFP-positive neurons immunostained for GAP-43 (red); after treatment
1112 with control medium (left) or with Lasso-D (right). Right. Quantification of the total neurite length
1113 in GFP-expressing neurons after the treatment (t-test: non-significant, $p > 0.05$, $n = 30$ cells
1114 without Lasso-D and 61 cells with Lasso-D from 3 independent cultures).

1115

1116 **Figure 6**

1117 **Interaction of LPHN1 with soluble Lasso causes LPHN1 aggregation.** A. A scheme of
1118 behavior of LPHN1 fragments at rest (left) and after binding an active agonist (middle) or a non-
1119 agonistic antibody (right). B-D. Distribution of NTF and CTF in NB2a cells stably expressing
1120 LPHN1 and treated with control buffer (B), Lasso-D (C) or LTX^{N4C} (D). E. The binding of a non-
1121 agonistic antibody against NTF of LPHN1 does not cause an association of the NTF and CTF of

1122 LPHN1. Images shown are representative of 4 independent experiments ($n = 4-7$). All scale bars
1123 are in μm . **F.** Quantitative analysis of correlation between the ligand-induced redistribution of NTF,
1124 CTF and ligand. T-test with Bonferroni correction: **, $p < 0.01$; ***, $p < 0.001$; $n = 4-7$ independent
1125 experiments.

1126

1127 **Figure 7** with 1 supplement

1128 **Soluble Lasso induces Ca^{2+} signaling in LPHN1-expressing cells and enhances**
1129 **spontaneous exocytosis at neuromuscular junctions.** A. Changes in intracellular Ca^{2+}
1130 concentration in neuroblastoma cells stably expressing LPHN1 were monitored using a Ca^{2+}
1131 indicator dye, Fluo-4. The scheme of the experiment is shown in Figure 7—figure supplement 1,
1132 A. After 5 min recording of baseline fluorescence, the cells were treated (maroon arrowhead) with
1133 control buffer, 1 nM LTX^{N4C} or 360 nM Lasso-D. 20 min later, 2 mM Ca^{2+} was added (gray
1134 arrowhead) to synchronize the intracellular Ca^{2+} signaling, followed by 1 nM wild-type α -latrotoxin
1135 (open arrowhead) to measure F_{max} , for normalization. Left, profiles of normalized Fluo-4- Ca^{2+}
1136 fluorescence over time for the three conditions used (mean values \pm SEM are shown; the data are
1137 from 80-120 individual cells from $n = 4$ independent experiments). Right, integration of Fluo-4-
1138 Ca^{2+} fluorescence over time (from B). Pre-treatment with Lasso-D potentiates intracellular Ca^{2+}
1139 signaling. T-test with Bonferroni correction: *, $p < 0.05$; ***, $p < 0.001$. B. Experiments testing the
1140 effect of Lasso-D on the time-course of LTX^{N4C} -induced LPHN1-dependent Ca^{2+} signaling. Cells
1141 expressing LPHN1 were loaded with Fluo-4 and stimulated first with control buffer (black
1142 arrowhead, left) or 1.5 nM Lasso-D (maroon arrowhead, right), and then with 2 nM LTX^{N4C} (blue
1143 arrowhead). 1 nM wild-type LTX was added at the end (open arrowhead). Ca^{2+} fluorescence
1144 measurements were obtained as in A. Representative normalized Ca^{2+} fluorescence profiles are
1145 shown. C. Time delay before the onset of LTX^{N4C} -induced signaling in cells pretreated with control

1146 buffer or Lasso-D determined from traces in B. T-test: *, $p < 0.05$; the data are from 166 buffer-
1147 LTX^{N4C}-treated cells and from 144 Lasso-LTX^{N4C}-treated cells, from $n = 5$ independent
1148 experiments. D. Representative raw recordings of MEPPs in neuromuscular preparations from
1149 LPHN1 WT and KO mice, in buffer containing 2 mM Ca²⁺ without any agonists or in the presence
1150 of 20 nM Lasso-G or 1 nM LTX^{N4C}. E. The frequency of MEPPs in the absence or presence of 20
1151 nM Lasso-G, as in D. Left, Lasso-G significantly increases the frequency of MEPPs at
1152 neuromuscular junctions from WT mice, but has no effect on exocytosis in LPHN1 KO synapses.
1153 The data shown are the means \pm SEM from 21 (control) and 23 (Lasso-G) individual muscle fibers
1154 from 5 WT preparations and 36 and 26 muscle fibers from 6 KO preparations. Right, positive
1155 control: 1 nM LTX^{N4C} increases the frequency of MEPPs in WT, but not in LPHN1 KO
1156 neuromuscular junctions. The data are the means \pm SEM from 21 and 32 individual muscle fibers
1157 from 6 WT preparations and 36 and 12 muscle fibers from 6 KO preparations. Mann-Whitney test
1158 with Bonferroni correction for multiple comparisons: *, $p < 0.05$; **, $p < 0.01$; ***, $p < 0.001$; NS,
1159 non-significant.

1160 **Figure 7—figure supplement 1**

1161 **Design of the experiments testing Lasso induced Ca²⁺ signaling in LPHN1-expressing cells**
1162 **and its presynaptic action at mouse neuromuscular junctions. A.** Experimental paradigm for
1163 testing the effect of Lasso-D on LPHN1-dependent Ca²⁺ signaling. After 5 min recording of
1164 baseline fluorescence of neuroblastoma cells expressing LPHN1, the cells were treated with
1165 control buffer (gray arrowhead), 1 nM LTX^{N4C} (black arrowhead) or 360 nM Lasso-D (maroon
1166 arrowhead). 20 min later 2 mM Ca²⁺ was added (gray arrowhead) to synchronize the intracellular
1167 Ca²⁺ signaling, followed by 1 nM wild-type α -latrotoxin (open arrowhead) to induce maximal Ca²⁺
1168 influx through the LTX pore. **B.** Experimental paradigm for testing the effect of Lasso-D on the
1169 time-course of LTX^{N4C}-induced LPHN1-dependent Ca²⁺ signaling. Cells expressing LPHN1 were
1170 loaded with Fluo-4 and stimulated first with control buffer (black arrowhead) or 1.5 nM Lasso-D

1171 (maroon arrowhead), and then with 2 nM LTX^{N4C} (blue arrowhead). 1 nM wild-type LTX was added
1172 at the end (open arrowhead). **C.** Analysis of the amplitudes of MEPPs recorded at neuromuscular
1173 junctions from WT and KO mice, indicating a lack of **postsynaptic** effects of Lasso-G or LTX^{N4C}.
1174 **Left**, the mean amplitudes of MEPPs in the absence or presence of Lasso-G. The data are the
1175 means \pm SEM from 21 (control) and 23 (Lasso-G) individual muscle fibers from 5 WT preparations
1176 and 36 and 26 muscle fibers from 6 KO preparations. **Right**, the mean amplitudes of MEPPs in
1177 the absence or presence of 1 nM LTX^{N4C}. The data are the means \pm SEM from 21 and 32
1178 individual muscle fibers from 6 WT preparations and 36 and 12 muscle fibers from 6 KO
1179 preparations. Mann-Whitney test with Bonferroni correction for multiple comparisons: NS, non-
1180 significant.

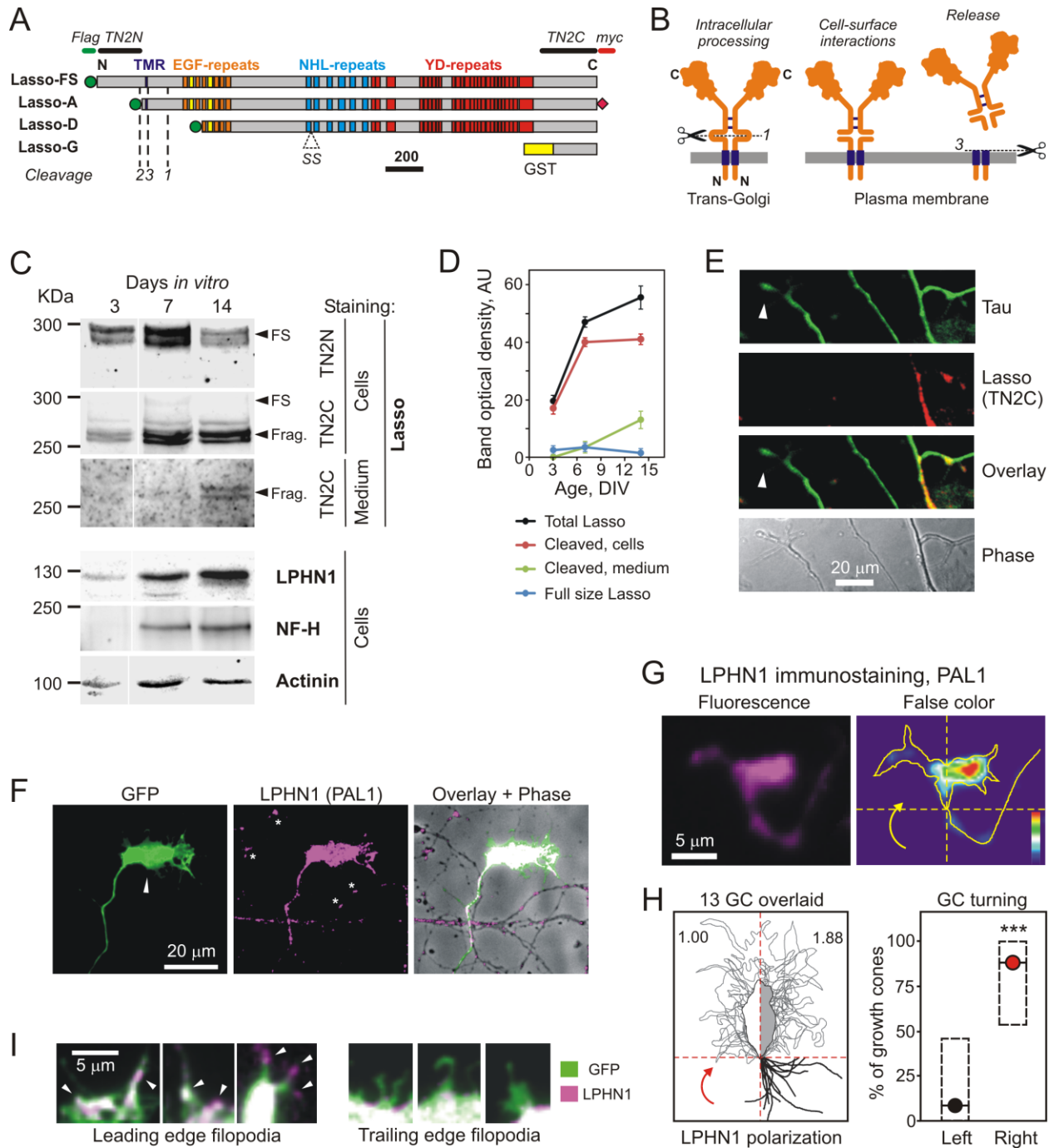
1181

1182 **Figure 8**

1183 **A proposed scheme of the mechanism of axonal attraction by released Lasso ECD.** When
1184 Lasso binds the NTF of LPHN1, it causes its re-association with the CTF. This activates $G\alpha_{q/11}$
1185 and triggers the PLC signaling cascade. Downstream of this cascade, the local IP₃-induced
1186 calcium release (IICR) from intracellular stores stimulates exocytosis and may also stimulate
1187 reorganization of actin through Ca²⁺/calmodulin-dependent protein kinase II (CaMKII), thus
1188 mediating axonal attraction. The dashed line represents LPHN1-mediated activation of neuronal
1189 adhesion molecules via an unknown mechanism that may lead to axonal fasciculation observed
1190 in the presence of soluble Lasso (Figure 5C, F).

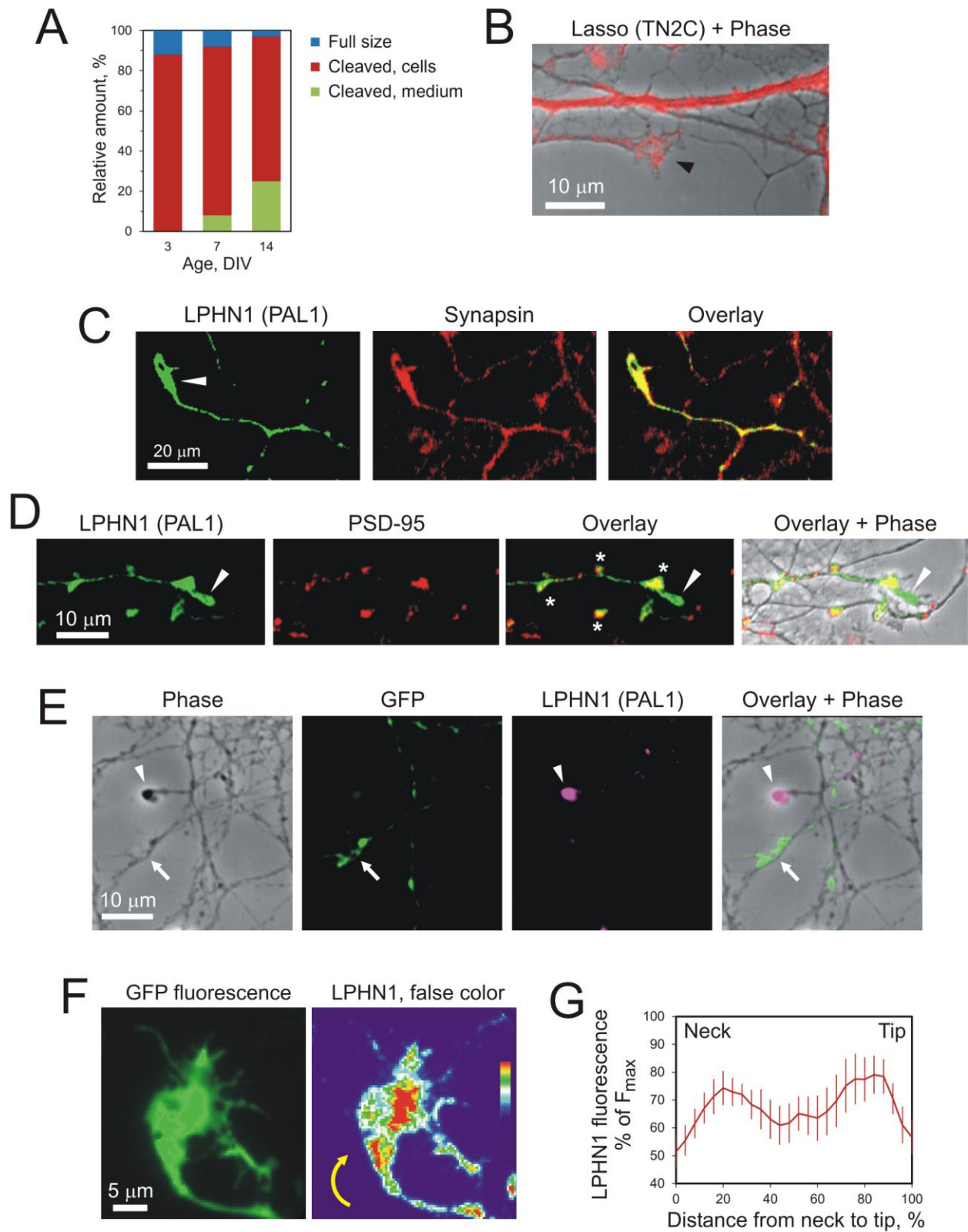
1191

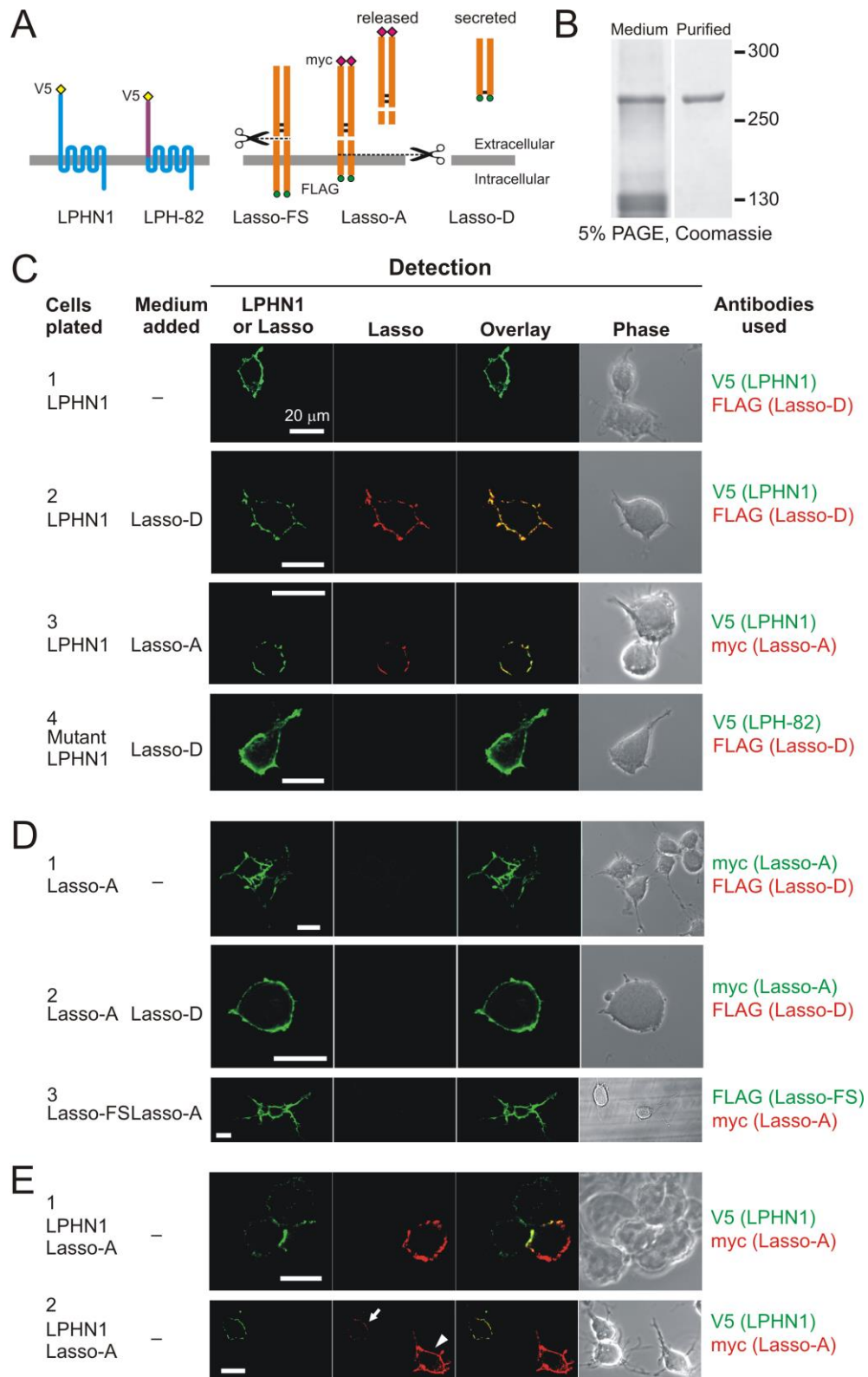
1192 Figure 1

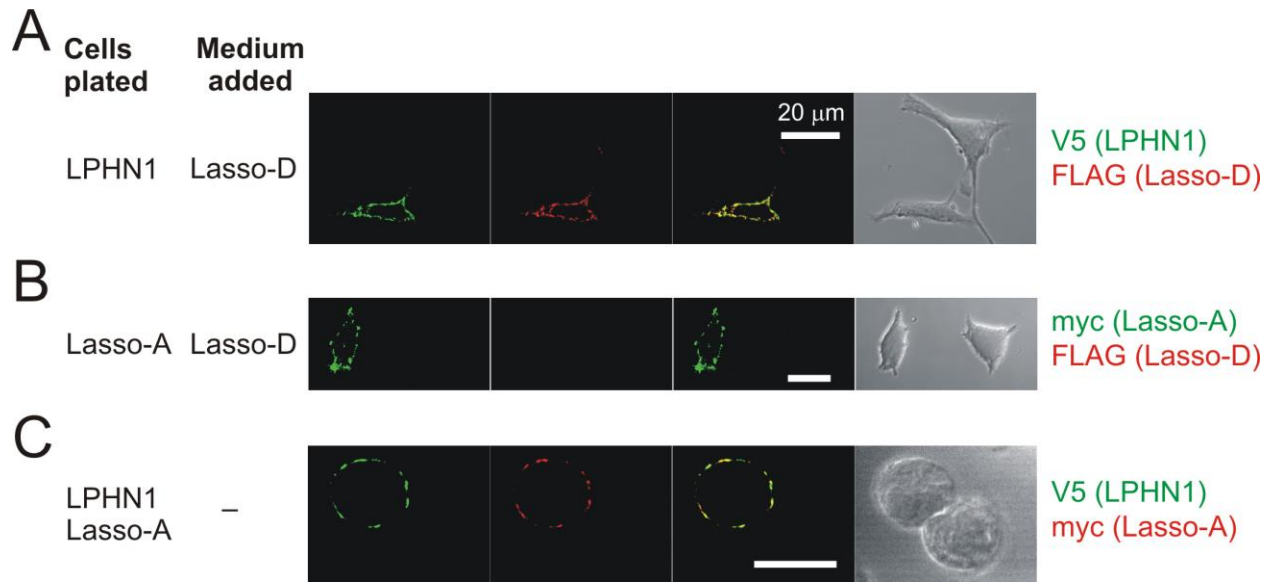


1193

1194

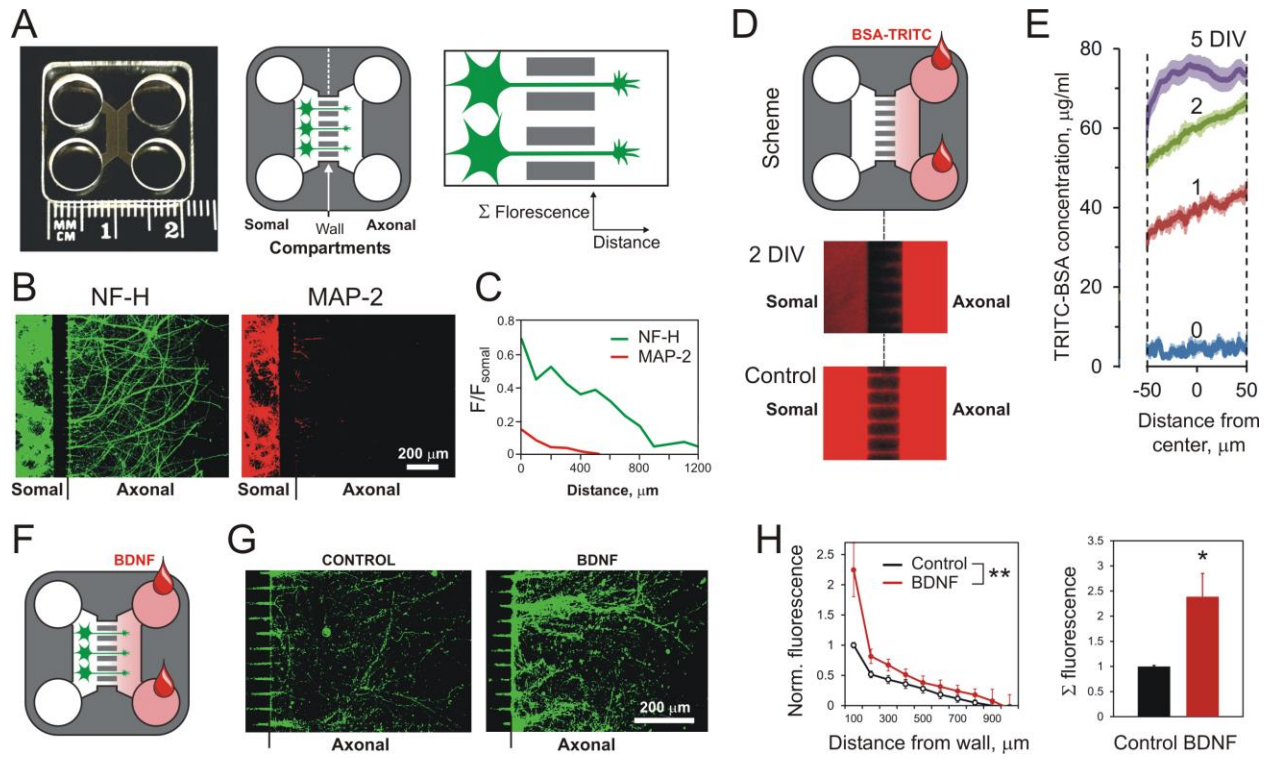






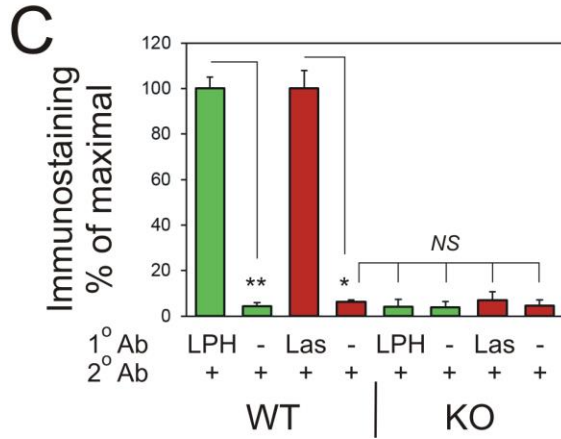
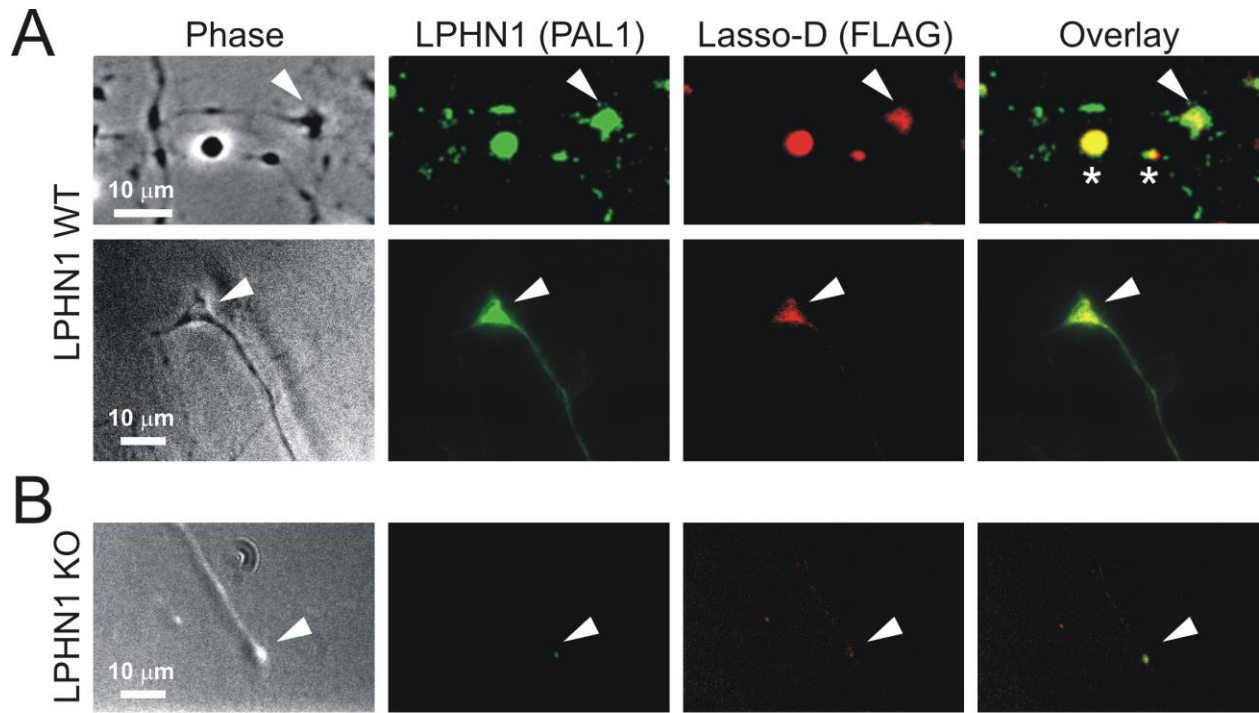
1200

1201



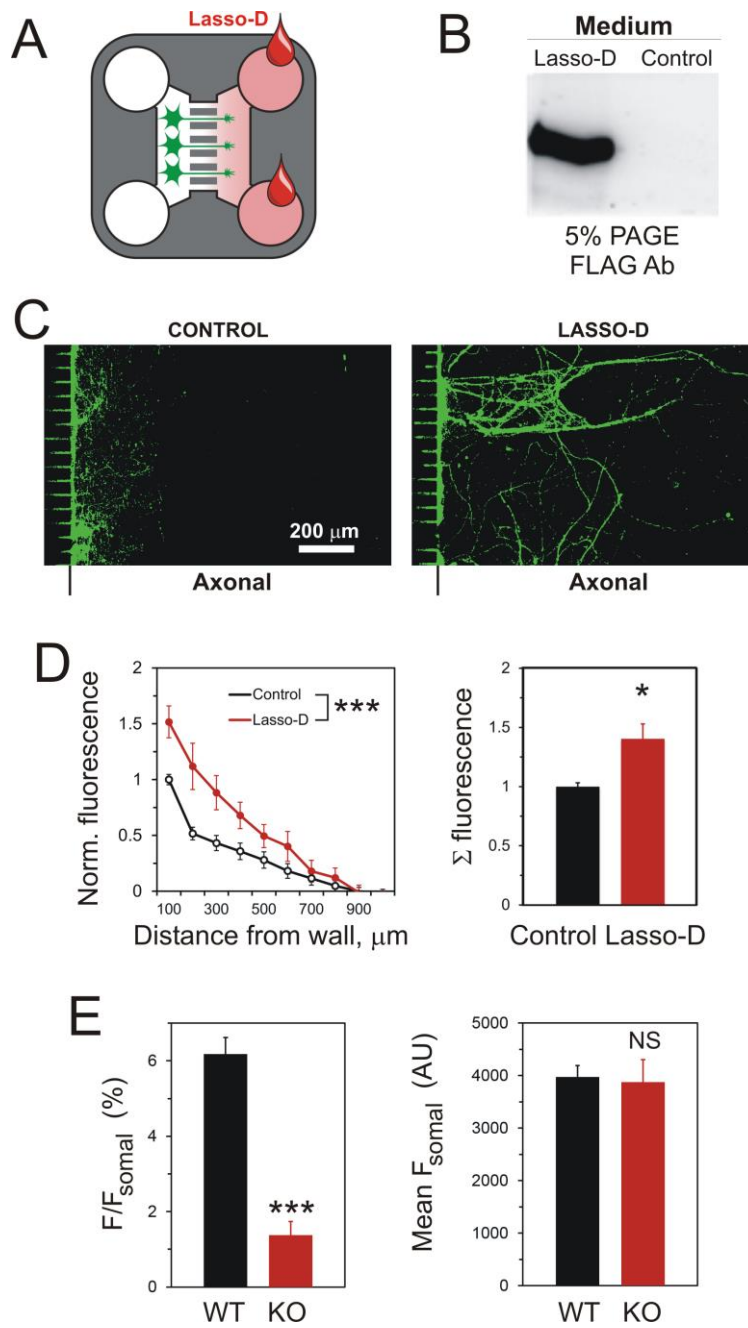
1203

1204



1206

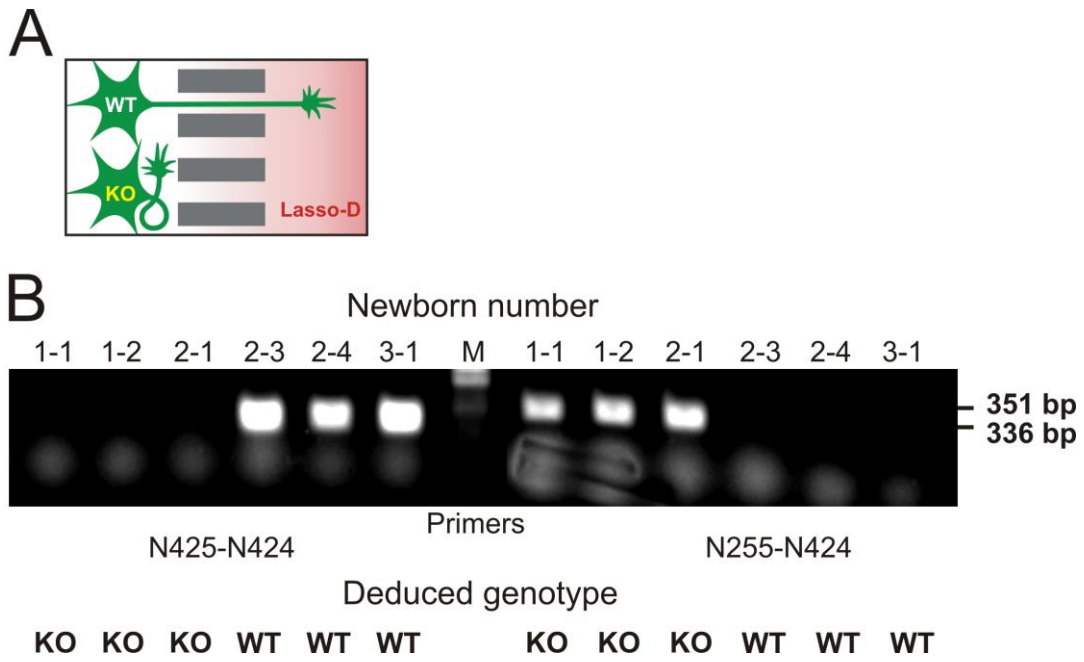
1207



1209

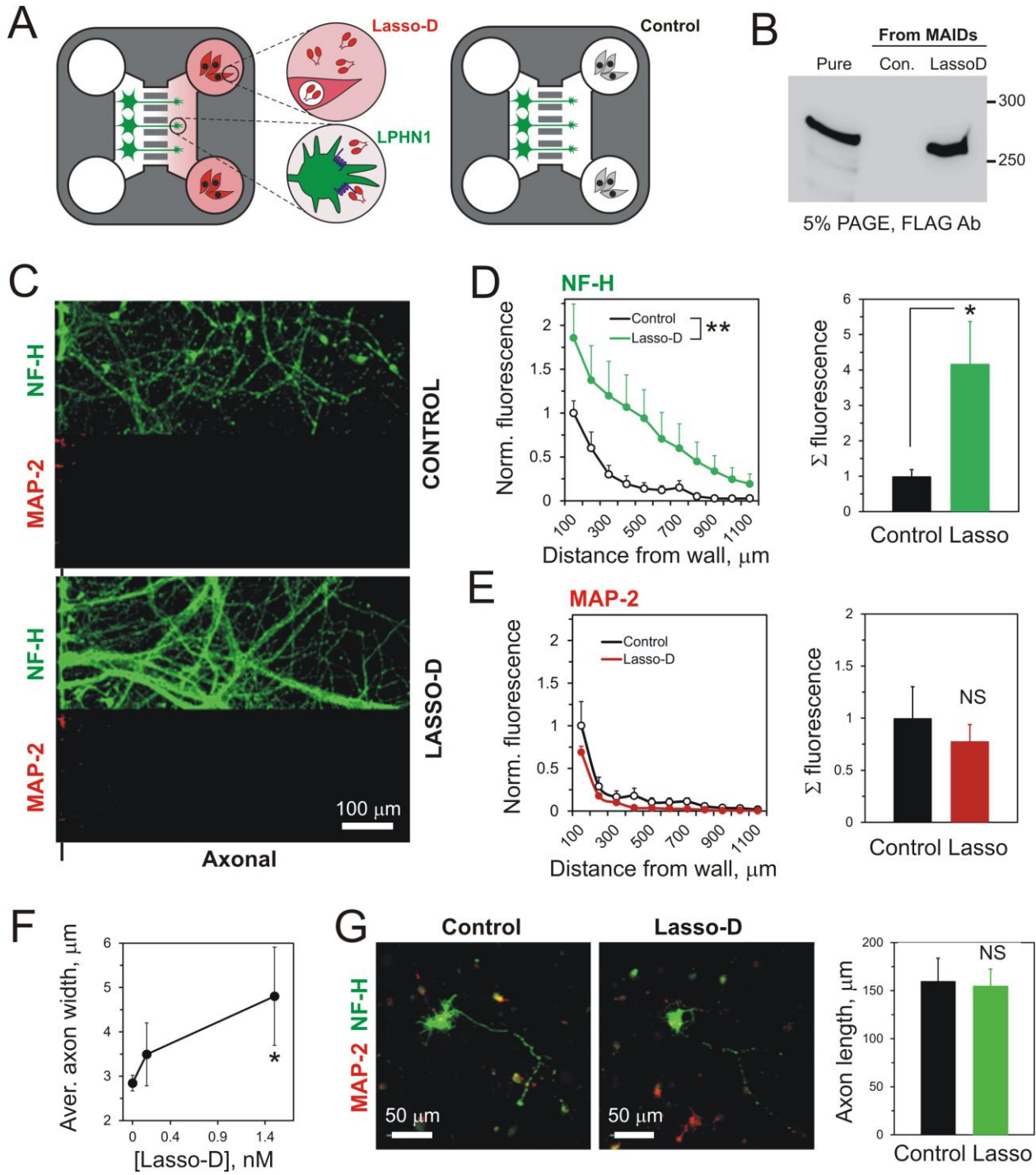
1210

1211 Figure 4 – Figure supplement



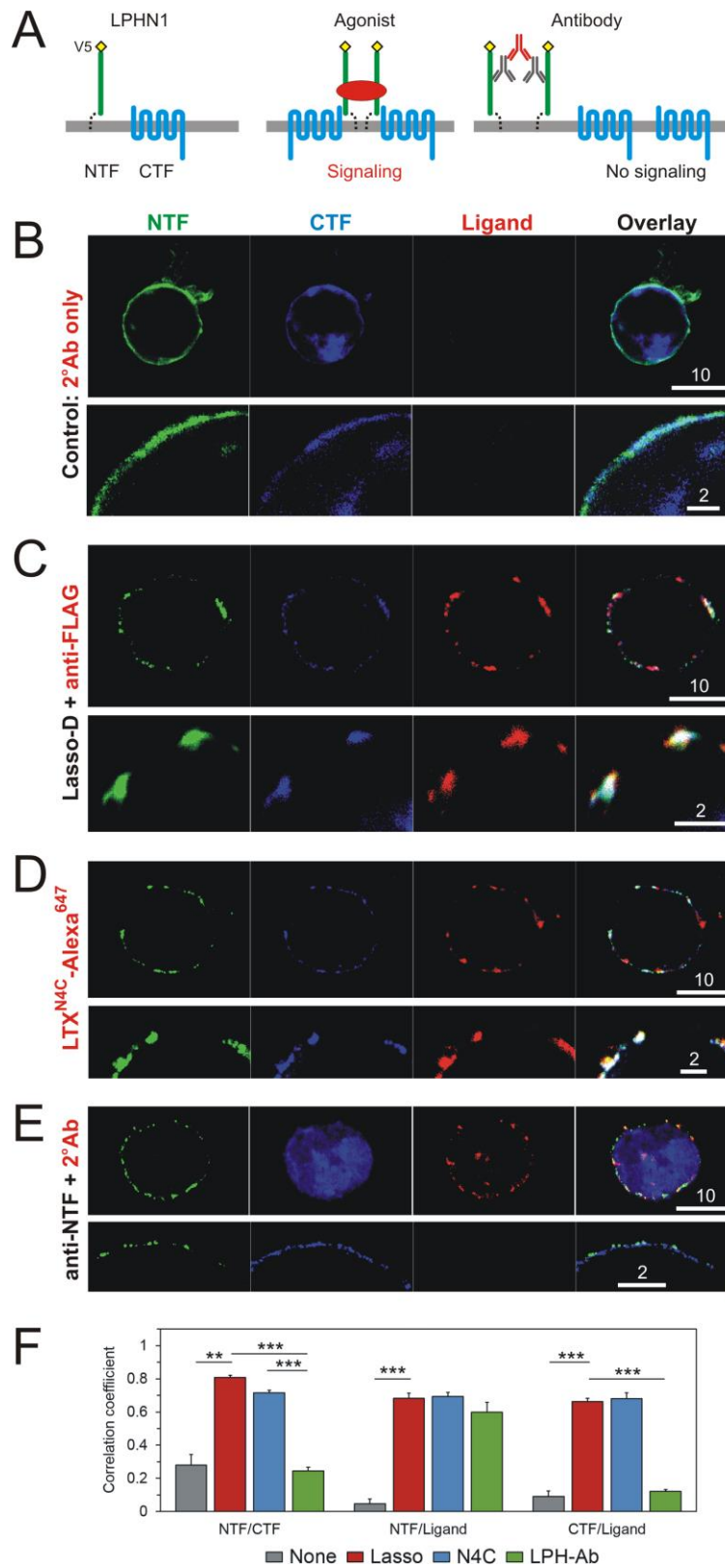
1212

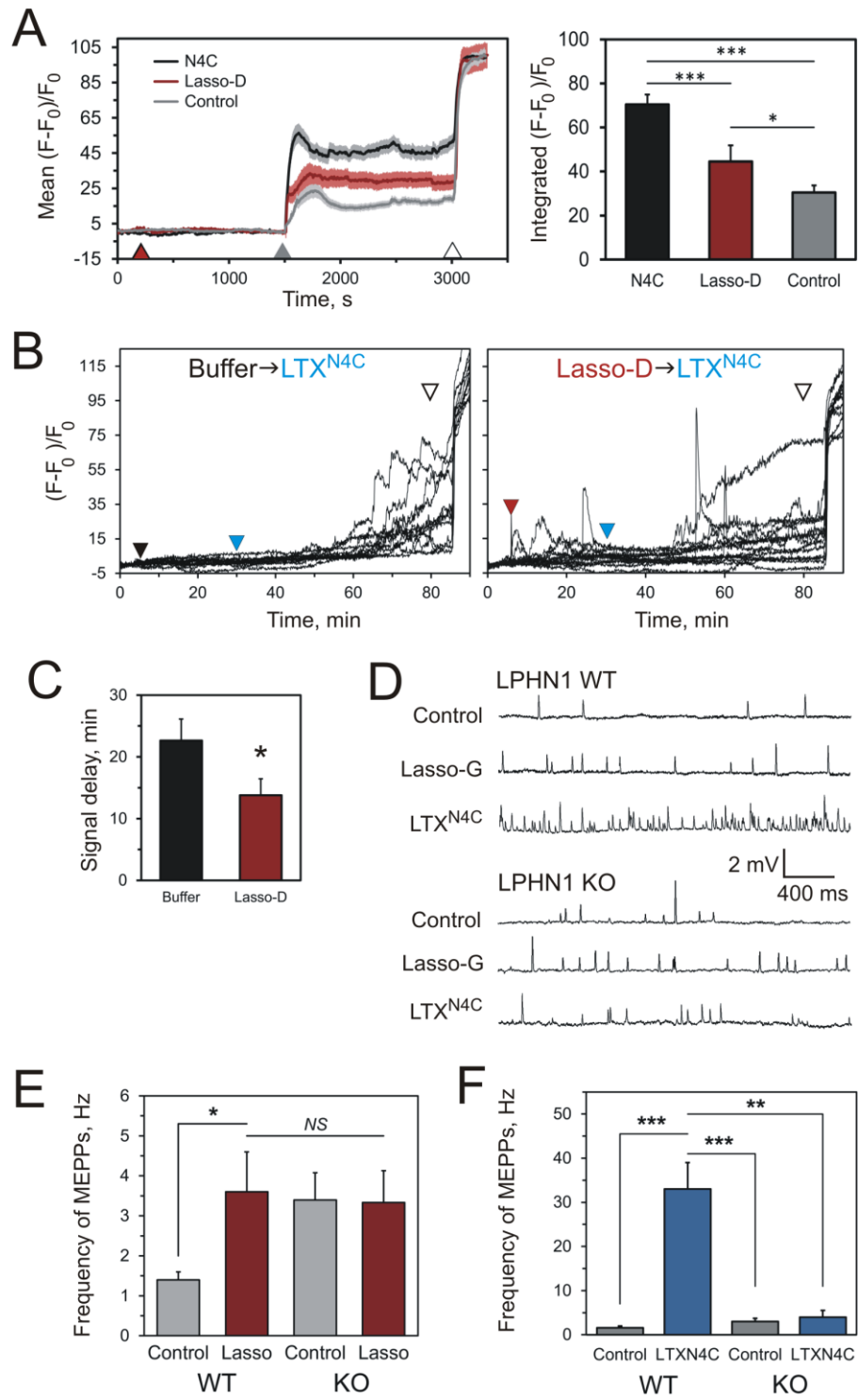
1213



1215

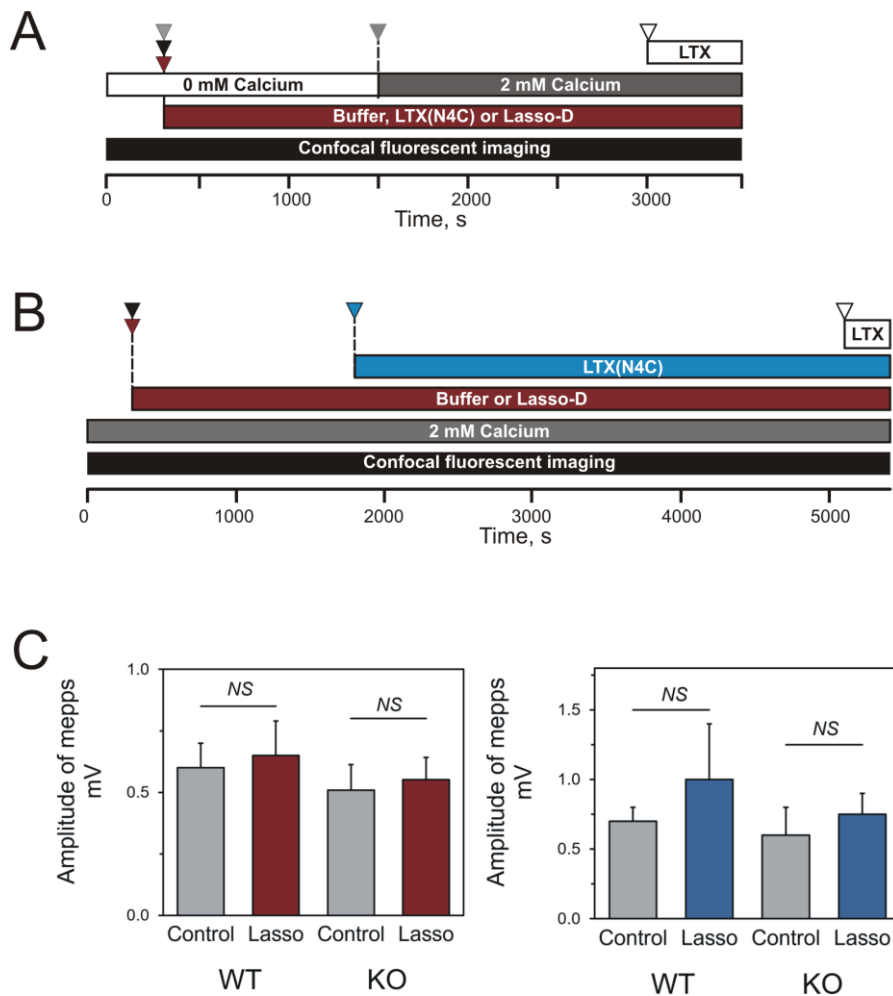
1216





1220

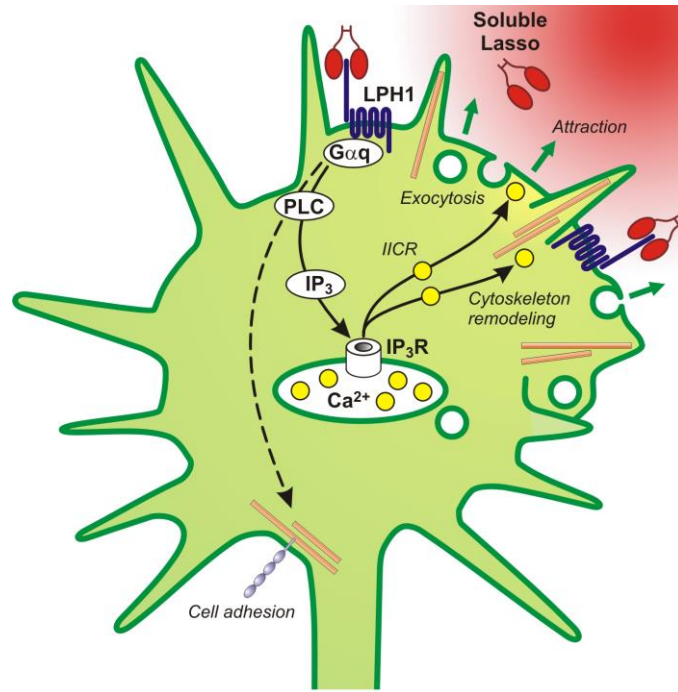
1221



1223

1224

1225 Figure 8



1226